Environmental Earth Sciences (2026) 85:170
https://doi.org/10.1007/s12665-026-12885-6

ORIGINAL ARTICLE

Performance assessment of 22 CMIP6 climate models for projecting wind climate and wind power over the Mediterranean Sea

Emre Çalışır[1] · Khalid Amarouche[1] · Recep Emre Çakmak[1] · Adem Akpınar[1]

Received: 19 July 2025 / Accepted: 20 February 2026
© The Author(s) 2026

Abstract

This study aims to (1) evaluate the spatial accuracy of 22 CMIP6 climate models in simulating wind climate over the Mediterranean Sea, (2) assess their performance in estimating wind power density across different wind conditions using percentile-based analysis, and (3) examine near-term projected wind climate changes under different SSP scenarios. The models were selected based on the availability of 3-hourly near-surface wind data (10 m height) for historical (1985–2014) and near-term (2015–2024) periods under four SSP scenarios (SSP1-2.6, SSP2-4.5, SSP3-7.0, SSP5-8.5) with consistent spatial coverage. The comparison metrics used to compare CMIP6 individual model output against ERA5 reanalysis data are the bias and the normalized bias supported by statistical test to evaluate the related confidence intervals. The best-performing models were identified based on their ability to reproduce both the long-term average and variability of historical wind speeds with low bias and narrow confidence intervals. Furthermore, a percentile-based evaluation (5th to 95th) was conducted to assess model accuracy across the full range of wind conditions, from calm to high-energy periods, ensuring reliable projections of future wind power density distribution changes. The results show statistically significant differences in model performance across sub-basins, with EC-Earth3 emerging as the most accurate and consistent model for most regions, maintaining normalized differences within ±0.2 for most percentiles (e.g., Aegean Basin St.11, Alboran Basin St.1). EC-Earth3 demonstrates balanced performance across all wind conditions, while CNRM-CM6-1-HR tends to overestimate wind power density at higher percentiles, particularly in the Balearic Basin (St.2, ~0.2–0.6) and Tyrrhenian Basin (St.6, ~0.6–0.8). Near-term projections (2015–2024) across four SSP scenarios evaluated through linear trend analysis show partial agreement between ERA5 and EC-Earth3, particularly under SSP5-8.5, but significant regional discrepancies elsewhere. This study provides sub-basin-specific guidance for climate model selection in Mediterranean wind resource assessments, supporting renewable energy planning and climate adaptation strategies.

Keywords Winds · Wind Energy · Climate Change · CMIP6 · EC-Earth3 · Mediterranean Sea

Introduction

The Mediterranean Sea (Med Sea) has often been considered as a climate change hot spot (Tuel and Eltahir 2020). The geographical location of the Med Sea exposes it to most of global teleconnection climate patterns. In term of offshore wind-wave climate, variations are primarily driven by atmospheric pressure systems and synoptic-scale circulation patterns, including the Scandinavia Pattern (SCA), the East Atlantic/West Russia Pattern (EA/WR), the NAO Pattern, and the East Atlantic Pattern (EA), which modulate wind intensity and direction through shifts in pressure gradients and storm tracks (Lionello and Scarascia 2018; Nissen et al. 2010). Additionally, regional processes such as orographic channeling, land-sea thermal contrasts (Drobinski et al.

✉ Emre Çalışır
emrecalisir@uludag.edu.tr

Khalid Amarouche
khalidamarouche@uludag.edu.tr

Recep Emre Çakmak
remrecakmak@uludag.edu.tr

Adem Akpınar
ademakpinar@uludag.edu.tr

[1] Department of Civil Engineering, Bursa Uludağ University, Gorukle Campus, Bursa, Turkey

Published online: 18 March 2026

2014; Lionello et al. 2006), and the influence of cyclogenesis in the western Mediterranean (Campins et al. 2011; Trigo et al. 1999), further shape the wind field variability across different sub-basins. The Med Sea region is also known for its climate change awareness due to water scarcity, for the concentration of economic activities in coastal areas, and for its dependence on climate-sensitive agriculture (Cos Espuna 2021; IPCC, 2001). Considering the complex orographic and geomorphological aspect of the Med Sea, it is considered as challenging for the wind forecast models compared to open oceans. The study of wind and wave climate in the Med Sea often requires a careful selection of appropriate wind models. At present, a significant number of global climate models (GCMs) providing wind climate simulations are available for use in climate change studies. Different scenarios for the future projections are presented by the World Climate Research Program (WCRP) under the Intergovernmental Panel on Climate Change (IPCC). The IPCC models based on the Coupled Model Inter-comparison Project phase 3 (CMIP3) and CMIP5 have been used in several studies (Barcikowska et al. 2020; Çakmak et al. 2022; Cramer et al. 2018; Kamranzad and Mori 2019; Lemos et al. 2020; Lobeto et al. 2023; Reyers et al. 2016; Samuels et al. 2018; Semedo et al. 2012) to investigate the climate change impacts on wind and wave climate all around the world and for different disciplines (i.e. ecology, atmospheric chemistry, meteorology) (Krishnan and Bhaskaran 2020). CMIP6 climate models are the newest set of global historical and future projections (Eyring et al. 2016). Unlike CMIP5 models that utilized Representative Concentration Pathways (RCPs), these new generations of GCM models consider the Shared Socio-economic Pathways (SSP) for future projections with improvements in detecting future changes (Eyring et al. 2016; Stouffer et al. 2017). SSPs offer a more realistic approach by combining various alternative socio-economic predictions (e.g., population, Gross Domestic Product (GDP), technological development) with future climate radiation forcing (Gidden et al. 2019). While CMIP5 scenarios were created with RCPs with different forcing levels (2.6, 4.5, 6.0, 8.5), CMIP6 utilizes seven SSP-based scenarios with radiative forcing ranging from 1.9 to 8.5 W/m² by the end of the 21 st century: SSP1-1.9, SSP1-2.6, SSP2-4.5, SSP3-7.0, SSP4-3.4, SSP4-6.0, and SSP5-8.5 (O'Neill et al. 2016). There are several studies (Kamranzad et al. 2020a, b; Lemos et al. 2023) evaluating CMIP6 models on a global scale. However, CMIP6 models have been less investigated in the Mediterranean Sea. Previous studies (Carvalho et al. 2017; Gumuscu et al. 2024; Rusu 2024) on the impact of climate change on wind climate and energy in the Mediterranean region have generally been conducted with CMIP5 and different RCP scenarios. Recent Mediterranean studies have utilized CMIP5-driven regional simulations for wave projections (Toomey et al. 2025) or single regional climate models focusing on maritime transport routes and wave conditions (Chirosca and Rusu 2025; Rusu 2025). Regarding CMIP6 climate model simulations, Carvalho et al. (2021) analyzed the future changes in wind speed (WS) and wind power density (WPD) over Europe. They used a multi-mean ensemble of fifteen global climate models, two different future periods and two different scenarios (SSP2-4.5 and SSP5-8.5). The evaluation was performed for the multi-mean ensemble models compared to ERA5 reanalysis data, however the evaluation of the individual models was not presented. Akinsanola et al. (2021) evaluated the performance of fourteen global climate models and their ensemble model against the ERA5 wind reanalysis for future wind climate projection in south western part of Africa. Martinez and Iglesias (2023) presented and evaluated an ensemble derived by nine different CMIP6 global climate models and considering three different future scenarios (SSP1-2.6, SSP2-4.5, and SSP5-8.5). The evaluation was performed for the ensemble model against ERA5 reanalysis, but no evaluation was presented for the individual models. Claro et al. (2023) examined the wind energy potential of the Portuguese coast and mainland with a multi mean ensemble using nine different CMIP6 global climate model members and future assessments were made with the SSP5-8.5 scenario in two different future periods. They only evaluated the multi-model ensemble against ERA5 reanalysis. While Lira-Loarca et al. (2021) evaluated future wind and wave energy resources in the Mediterranean using EURO-CORDEX regional climate projections focusing on combined exploitability metrics, their study did not systematically assess the performance of underlying CMIP6 global climate models. Previous CMIP5-based studies focused on single-model assessments in specific regions outside the Mediterranean (e.g., Hdidouan and Staffell 2017 for UK waters; Neill 2024 for the Irish Sea), lacking basin-wide systematic evaluation frameworks. Barbariol et al. (2021) provided an excellent ERA5-based climatology of historical Mediterranean wave climate, but our work focuses on a different objective: systematically evaluating and identifying the most accurate CMIP6 climate models against ERA5 reanalysis. Most existing regional studies on wind climate projections derived from CMIP6 are based on multi-model ensembles of different models; however, the rationale for selecting ensemble members and their weighting schemes is rarely justified (Brunner et al. 2020; Sanderson et al. 2017), potentially introducing systematic biases and limiting the reliability of regional projections. Thus, to date, systematic evaluation of individual CMIP6 wind model performance across the entire Mediterranean Sea and its sub-basins has not been conducted, with existing studies primarily focusing on ensemble-mean projections. Çetin et al. (2024)

established a machine learning based ensemble model using 28 different CMIP6 global climate models for Türkiye. The ML based ensemble model was evaluated using MERRA2 and ERA5 datasets in geographical regions on the Turkish mainland. This method may allow the definition of the right weight of each model in the ensemble model; however, it does not show the accuracy of the individual models and do not cover the Med Sea.

Given the study background, there is a lack of research evaluating the historical performance considering the uncertainty associated with CMIP6 wind simulations over the Mediterranean Sea. This study aims to assess the wind accuracy of 22 CMIP6 climate models (selected based on the availability of 3-hourly near-surface wind data at 10 m height for both historical (1985–2014) and future SSP scenario periods (2015–2024) with consistent spatial coverage over the Mediterranean Sea) to determine the best fit wind climate model for wind speed and wind energy projection in comparison with the ERA5. While high-resolution Regional Climate Models (RCMs) offer advantages in resolving land-sea transitions and coastal processes, this study focuses on Global Climate Models (GCMs) from CMIP6 for several reasons: (1) CMIP6-driven regional downscaling products (e.g., CORDEX-CMIP6) were not yet fully available for the Mediterranean basin at the time of this study, (2) establishing CMIP6-GCM performance benchmarks is essential for future RCM validation and bias correction studies, as RCMs inherit uncertainties from their driving GCMs, and (3) establishing GCM performance benchmarks is essential for future RCM validation and bias correction studies, as RCMs inherit uncertainties from their driving GCMs. The use of accurate models enables the reduction uncertainty in both wind and wave climate change projections. While historical skill does not guarantee future accuracy due to potential non-stationarity in climate dynamics, models demonstrating strong performance in reproducing observed variability provide a more credible basis for projecting future changes (Knutti et al. 2010). Furthermore, knowing the accuracy of wind climate models can enable better identification of individual models and weighting to be considered to develop a more robust multi-modal ensemble for climate change studies. Multi-model ensembles typically outperform individual models by averaging out model-specific biases (Tebaldi and Knutti 2007); however, performance-weighted ensembles can further enhance projection reliability by emphasizing more accurate models (Brunner et al. 2020). For this purpose, the historical performance (1985–2014) of 22 different CMIP6 GCMs was evaluated against ERA5 reanalysis data across the entire Mediterranean Sea and its sub-basins. Considering the model performance varies significantly across different spatial scales (i.e., a model may exhibit high accuracy in one sub-basin but poor accuracy in another), wind model performance was assessed separately for the Med sub-basins. Furthermore, the models with the best accuracy over the whole Mediterranean Sea are identified, and their uncertainties over the historical period are analyzed. The uncertainty of the models in all percentiles from extremely low to extremely high values was analyzed at the stations determined to cover all basins. The results of this study provide an overall view of the uncertainties related to the model accuracy and the large differences between the climate models. By presenting the wind performance of the climate models based on sub-locations, the researchers may consider the most adequate models based on the area of interest. Furthermore, the best-performing models identified from historical evaluation may be considered to build a more robust multimodal ensemble for future projections of wind climate and offshore wind energy. In the second part of this study, the best-performing model identified from the historical evaluation was further assessed for its near-term annual mean wind speed projections (2015–2024) under four different SSP scenarios (SSP1-2.6, SSP2-4.5, SSP3-7.0, and SSP5-8.5). The simulated wind speeds were compared against ERA5 annual mean wind reanalysis data for the same period to evaluate the model's capability to reproduce recent observed variability under different scenario forcings. This comparison aims to provide a diagnostic evaluation of the model's near-term performance rather than to identify a "best" or "most realistic" SSP scenario, acknowledging that differences in external forcing among SSPs during this period are minimal and largely within the range of internal climate variability (as discussed in IPCC AR6, Chap. 4). With the availability of near-term data (2015–2024) from CMIP6 under different SSP scenarios, it is now possible to assess how well these projections reproduce observed wind variability. Such an evaluation provides a diagnostic check of model performance and helps build confidence in the use of CMIP6 simulations for near-term wind climate studies, considering differences among SSPs are minimal over this short period.

Data

The present study evaluates 22 Global Climate Models (GCMs) featured in the CMIP6 project. Although there are many more climate model options out there, model selection is based on the following criteria: GCM should provide WSs at 10 m above sea level, the temporal resolution should be ≤ 3 h, and the model data set should contain future projections. Twenty-two GCMs meet these criteria to nowadays. Twenty-two GCMs that meet the specified conditions were taken from the CMIP6 category (ESGF, 2024).

For each model, the variant label follows the CMIP6 naming convention: r#i#p#f#, where 'r' denotes the realization (ensemble member), 'i' the initialization method, 'p' the physics parameterization, and 'f' the forcing variant. We prioritized the r1i1p1f1 variant following CMIP6 standardization protocols (Eyring et al. 2016; Juckes et al. 2020). When r1i1p1f1 was unavailable in the ESGF archive (January 2024), we selected the next available forcing variant (f2 or f3) while strictly maintaining r1i1p1, as the ensemble member (r), initialization (i), and physics configuration (p) parameters directly affect model behavior, whereas the forcing index (f) primarily denotes technical variations in external forcing datasets without changing model physics (Juckes et al. 2020). This approach ensured consistent ensemble member and physics configuration across all models while accommodating practical data availability constraints. The final variant distribution was: r1i1p1f1 (17 models, 77%), r1i1p1f2 (4 models, 18%), and r1i1p1f3 (1 model, 5%), as documented in Table 1. Table 1 provides an overview of the 22 CMIP6 climate models we used in this study, listing their institutions, spatial resolutions, model variants, and key references. Sharing this information helps give a clear picture of the range of models we evaluated and compared. The differences in spatial resolution, for

Table 1 The 22 CMIP6 climate models used in this study with institutional information, spatial resolutions, and variant specifications

Model	Institute	Nominal Resolution (km)	Native Resolution (lat x lon)	Variant	References
ACCESS-CM2	Commonwealth Scientific and Industrial Research Organization	250	1.25° · 1.875°	r1i1p1f1	(Dix et al. 2019)
AWI-CM-1-1-MR	Alfred Wegener Institute, Helmholtz Centre for Polar and Marine Research	100	0.935° · 0.9375°	r1i1p1f1	(Semmler et al. 2018)
BCC-CSM2-MR	Beijing Climate Center	100	1.1213° · 1.125°	r1i1p1f1	(Xin et al. 2018)
CMCC-CM2-SR5	Fondazione Centro Euro-Mediterraneo sui Cambiamenti Climatici, Lecce, Italy	100	0.9424° · 1.25°	r1i1p1f1	(Lovato and Peano 2020)
CMCC-ESM2		100	0.9424° · 1.25°	r1i1p1f1	(Peano et al. 2020)
CNRM-CM6-1	Centre National de Recherches Meteorologiques, Centre Europeen de Recherche et de Formation Avancee en Calcul Scientifique, Toulouse, France	250	1.4004° · 1.4063°	r1i1p1f2	(Voldoire 2018)
CNRM-CM6-1-HR		100	0.4993° · 0.5°	r1i1p1f2	(Voldoire 2019)
EC-Earth3	EC-Earth consortium, Rossby Center, Swedish Meteorological and Hydrological Institute/SMHI, Norrkoping, Sweden	100	0.7017° · 0.7031°	r1i1p1f1	(EC-Earth 2019)
GISS-E2-1-G	Goddard Institute for Space Studies, New York, NY, USA	250	2.0° · 2.5°	r1i1p1f2	(NASA/GISS, 2018)
HadGEM3-GC31-LL	Met Office Hadley Centre, Exeter, Devon, UK	250	1.25° · 1.875°	r1i1p1f3	(Ridley et al. 2019a)
HadGEM3-GC31-MM		100	0.5556° · 0.8333°	r1i1p1f3	(Ridley et al. 2019b)
IITM-ESM	Indian Institute of Tropical Meteorology Pune	250	1.9041° · 1.875°	r1i1p1f1	(Narayanasetti et al. 2019)
IPSL-CM6A-LR	Institut Pierre Simon Laplace, Paris, France	250	1.2676° · 2.5°	r1i1p1f1	(Boucher et al. 2018)
KACE-1-0-G	National Institute of Meteorological Sciences, Korea Meteorological Administration	250	1.25° · 1.875°	r1i1p1f1	(Byun et al. 2019)
KIOST-ESM	Korea Institute of Ocean Science and Technology, Busan, Republic of Korea	250	1.8947° · 1.875°	r1i1p1f1	(Kim et al. 2019)
MIROC6	Japan Agency for Marine-Earth Science and Technology, Atmosphere and Ocean Research Institute, The University of Tokyo, National Institute for Environmental Studies, RIKEN Center for Computational Science	250	1.4004° · 1.4063°	r1i1p1f1	(Shiogama et al. 2019)
MIROC-ES2L		500	2.7893° · 2.8125°	r1i1p1f2	(Tachiiri et al. 2019)
MPI-ESM-1–2-HAM	HAMMOZ-Consortium	250	1.8647° · 1.875°	r1i1p1f1	(Neubauer et al. 2019)
MPI-ESM1-2-HR	Max Planck Institute for Meteorology (MPI-M), Hamburg, Germany	100	0.9349° · 0.9375°	r1i1p1f1	(Gutjahr et al. 2019)
MPI-ESM1-2-LR		250	1.8647° · 1.875°	r1i1p1f1	(Brune et al. 2022; von Storch et al. 2017)
MRI-ESM2-0	Meteorological Research Institute, Tsukuba, Ibaraki, Japan	100	1.1213° · 1.125°	r1i1p1f1	(Yukimoto et al. 2019)
NESM3	Nanjing University of Information Science and Technology, Nanjing, China	250	1.8647° · 1.875°	r1i1p1f1	(Cao and Wang 2019)

example, can affect how well each model captures details of the wind climate across the Mediterranean sub-basins. Getting to know the variety and characteristics of these models is important for understanding the patterns of variability and biases we discuss in the results.

GCMs were evaluated between 1985 and 2014 for the historical period. For the near-term evaluation period (2015–2024), the best-performing historical model was further assessed under four SSP scenarios (SSP1-2.6, SSP2-4.5, SSP3-7.0, and SSP5-8.5) to identify which scenario projection shows the best agreement with ERA5 reanalysis data during this overlapping period.

The control dataset considered for the evaluation of the wind climate models is the ERA5 reanalysis from the ECMWF (Hersbach et al. 2020). The ERA5 is a new reanalysis product developed by ECMWF to replace ERA-Interim (Hersbach et al. 2018). These data, including a 10-member 4D-Var data assimilation ensemble with a resolution of 62 km, are produced by the Integrated Forecasting System (IFS) Cy41R2 (Dong et al. 2020). There are several approaches for calculating 10 m WSs in reanalysis datasets. In ERA5, a modified Monin-Obhukhov method is used to calculate the WS at 10 m (Pryor et al. 2009). ERA5 has a horizontal resolution of about ~31 km (0.25° × 0.25°) and a vertical resolution of up to 137 km with a temporal resolution of 1 h (Dong et al. 2020). WSs at 10 m above sea level between 1985 and 2014 were used in the study. It should be noted that ERA5, while being the most comprehensive reanalysis product available, is not equivalent to direct observations and contains inherent uncertainties arising from data assimilation processes, background model parameterizations, and observational data gaps in some regions (Hersbach et al. 2020). Nevertheless, ERA5 has been extensively validated against in-situ and satellite observations across global and regional scales (Belmonte Rivas and Stoffelen 2019) and represents the most reliable gridded wind dataset for climate model evaluation in the Mediterranean Sea.

Methodology

Data processing

In the present study, performance of wind speeds from 22 climate models are evaluated against winds of the ERA5 reanalysis to assess the uncertainty of the climate models, considering both the overall average and the performance over the wind speed distribution. Considering that GCMs have different spatial resolutions, as shown in Table 1, and that climate models are produced on a global scale, the climate data derived from each model simulations were first processed and adapted to the Med Sea region using Climate Data Operators (CDO) version 2.4.0 (Schulzweida 2023).

The first step was to downscale the global data to the Med Sea region using the bilinear interpolation operator 'remapbil', one of the CDO operators. In order to bring the data to a similar resolution as the ERA5 re-analysis dataset, a reduction was made to a spatial resolution of 0.25° x 0.25°. Longitude values are created from 7°W to 37°E with 177 steps, while latitude values are created from 29°N to 47°N with 73 steps. In order to get the temporal resolution of 3-hour time intervals in climate models on a similar scale to the ERA5 reanalysis model, the 'inttime' operator from CDO operators was used. This operator performs linear temporal interpolation between existing time steps, creating intermediate hourly values based on weighted averages of adjacent 3-hourly data points (Schulzweida 2023). The interpolation is only applied when both surrounding values exist; if both are missing, the result remains missing. Through this process, the 3-hour intervals were interpolated to 1-hour temporal resolution, ensuring temporal consistency with ERA5 data. At the end of the process, the data from each climate model between 1985 and 2014 were stored in different netCDF files on an annual basis.

Figure 1 shows the study area, and the reference points used in the study. The reference point selected at each location was placed in an open offshore site in the middle of each sub-basin. However, in sub-basins with a larger area, such as the southwestern Mediterranean basin and the Algerian basin, the position of the reference points was established in offshore areas likely to be exposed to wind depressions associated with other neighbor basins. For instance, station ST.4 is exposed to winds from the north, east, and west of the Algerian basin, while station ST.3 is not directly open to the western part of the Algerian basin, but rather to the Balearic basin. Station ST.7 was selected for its exposure to the western Mediterranean basins, while station ST.10 was selected for its location in the center of the southwestern basin and its exposure to the Ionian and Aegean basins. Station ST.12 was selected for its relative exposure to the Aegean Sea and to the eastern, southern, and northeastern wind fields.

In the comparisons of climate models with the ERA5 reanalysis dataset, the values over the sea were considered. In this context, downscaled climate models and ERA5 data were analyzed by excluding the areas over land.

Wind speed and power density calculations

Wind speeds were calculated from the surface u and v components of the WS at 10 m above sea level from climate models simulations and the ERA5 reanalysis for 30 years between 1985 and 2014. The long-term average wind

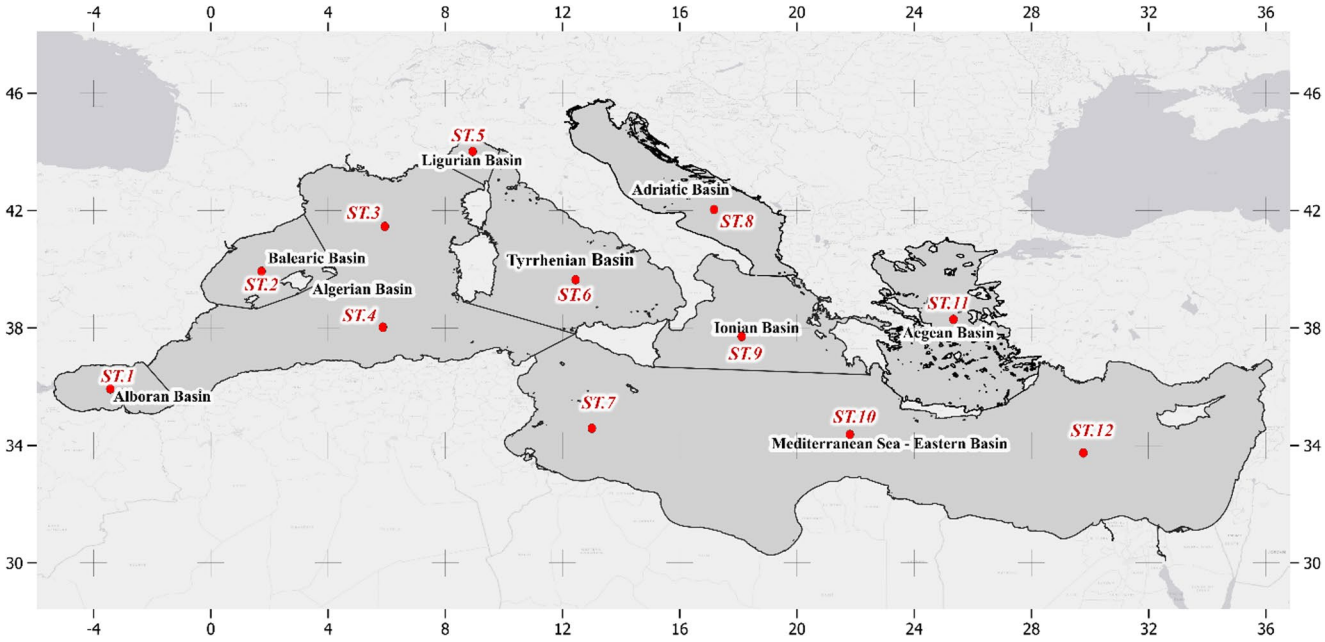


Fig. 1 Local Sub basins of Mediterranean Sea and reference locations used in this study

speed is the commonly used values in climate change studies (Çakmak et al. 2023; Dahunsi et al. 2025; Lobeto et al. 2021; Martinez and Iglesias 2023). An accurate estimate of historical changes allows to reduce the uncertainty related to model accuracy in future projections. The evaluation of wind model performance in estimating wind power density WPD was conducted in two steps. Firstly, the best-performing climate models for wind speed accuracy were identified based on spatial biases in WS obtained at different Mediterranean sub-basins. The biases are calculated for each grid point by subtracting the ERA5 WS average from each climate model WS average. Furthermore, the computed bias significance was tested using a student t-test with a confidence interval of 95%. The results obtained for each model are mapped and summarized considering the averaged absolute biases over the whole Mediterranean Sea and over 9 Mediterranean sub-basins. Secondly, the best-performing wind models were further evaluated by comparing their WPD values against ERA5 across the full percentile range (0th to 100th percentile) at 12 reference stations representing all Mediterranean sub-basins. This percentile-based distributional comparison reveals model performance not only at the median (50th percentile) but also across the entire range of wind conditions, from calm periods (lower percentiles) to extreme wind energy events (upper percentiles), providing a comprehensive assessment beyond mean-value comparisons.

The wind power density is computed based on wind speed and air density (Emeis 2013), where WPD is defined in Eq. 1 as follows.

$$WPD = \frac{1}{2}\rho V^3 \tag{1}$$

Here, V is the WS adjusted to the turbine center level. The WS height value used in this study is taken as 90 m. ρ is the air density value, and standard conditions are assumed with a constant value of 1.225 kg m^{-3}. While air density varies with temperature, pressure, and humidity, the use of a constant standard sea-level density is a widely accepted simplification in comparative wind resource assessments (Akpınar 2013; Carvalho et al. 2021; Martinez and Iglesias 2023). This approach ensures consistency across all climate models and focuses the evaluation on wind speed variability rather than introducing additional uncertainties from density calculations, which is appropriate for relative model performance comparison. In the WPD calculation, the WSs of the climate model and ERA5 data set obtained at a height of 10 m are considered to compute the WPD at the turbine center level height (estimated at 90 m) using the power law method defined in Emeis (2005) (Eq. 2) the WSs are approximated to the desired z height level.

$$WS(z) = WS(z_{ref})\left(\frac{z}{z_{ref}}\right)^{\alpha} \tag{2}$$

Here, z is the height of the turbine center, which is assumed to be 90 m. z_{ref} is the reference height, WS(z_{ref}) is the WS at the reference level, and α is the power law exponent. The power law exponent value was accepted as α = 1/7, which is suitable for open terrain surfaces and has been used

in previous studies (Akinsanola et al. 2017, 2021; Akpınar 2013; Sawadogo et al. 2019). We acknowledge that α can vary with atmospheric stability, wind direction, and local conditions; however, α = 1/7 represents a widely accepted approximation for neutral atmospheric conditions over offshore environments (Emeis 2013). This simplified approach is appropriate for comparative climate model evaluation, as it ensures consistency across all models and focuses on relative performance differences rather than absolute wind resource values. The use of a constant exponent is a common practice in large-scale wind climate assessments when detailed atmospheric stability data are not available from all climate models.

After evaluating the wind climate model based on historical data and identifying the best-performing model, the near-term projections was also assessed. This study employs two distinct evaluation periods with different objectives: (1) a 30-year historical period (1985–2014) for comprehensive wind climate model performance assessment and the best performing wind climate model selection, and (2) a 10-year near-term period (2015–2024) for scenario validation using four different SSP scenarios of the best-performing model identified from the historical evaluation. CMIP6 models use historical simulations up to the end of 2014 and transition to future scenarios from 2015 onwards. The projection is provided under different scenarios for the period between 2015 and 2100. However, given the availability of reanalysis data, only near-future projections can be effectively evaluated. The 30-year historical period provides a robust climatological basis for selecting and comparing wind climate models, in line with standard climate assessment practices. The subsequent 10-year evaluation serves a different purpose, which is to determine which Shared Socioeconomic Pathway (SSP) scenario of the best-performing model best aligns with observed trends early on, rather than establishing climatological means. For this purpose, the 10-year near-term period (2015–2024) is analyzed by comparing ERA5 reanalysis data with EC-Earth3 model projections under four different SSP scenarios (SSP1-2.6, SSP2-4.5, SSP3-7.0, and SSP5-8.5). The analyses are based on 12 reference points throughout the Mediterranean Sea, as shown in Fig. 1. For each reference station, annual means of WS and WPD from the ERA5 and EC-Earth3 datasets were used to construct time series. Linear regression analyses were then applied to these series to identify and quantify trends over the 10-year analysis period. This assessment provides the most accurate projection over the present period for both WS and WPD, which can be taken into account when assessing wind climate and wind energy in the coming years.

To perform the trend analysis, The Theil–Sen estimator (Sen 1968; Theil 1950) was used. This non-parametric method is based on Kendall's rank correlation and is robust against outliers and non-normal data distributions. Unlike the least squares estimator, it does not assume a normal distribution. In this approach, the slope between all possible pairs of data points (Y_i,t_i) and (Y_j,t_j) is calculated as:

$$a_{ij} = \frac{(Y_j - Y_i)}{(t_j - t_i)} \qquad with \;\; 1 < i < j < n \tag{3}$$

The Theil–Sen slope is then defined as the median of all a_{ij} values. In this study, the estimator was applied to annual wind data at each reference point over a 10-year period (2015–2024) for ERA5 data and EC-Earth3 evaluated SSPs.

The Mann–Kendall test (Kendall 1975; Mann 1945) was also used to evaluate the statistical significance of detected trends. This non-parametric test assesses whether a monotonic trend exists in a time series without assuming normality. The test statistic S is computed as:

$$\mathrm{S} = \sum_{i}^{n-1} \sum_{j}^{n} sgn\,(y_j - y_i) \tag{4}$$

where sgn(y_j – y_i) is an indicator function defined as

$$\begin{array}{ll} \mathrm{sgn}\,(\mathrm{X_j} - \mathrm{X_k}) = 1 & \text{if } \mathrm{X_j} - \mathrm{X_k} > 0 \\ \mathrm{sgn}\,(\mathrm{X_j} - \mathrm{X_k}) = 0 & \text{if } \mathrm{X_j} - \mathrm{X_k} = 0 \\ \mathrm{sgn}\,(\mathrm{X_j} - \mathrm{X_k}) = -1 & \text{if } \mathrm{X_j} - \mathrm{X_k} < 0 \end{array} \tag{5}$$

For the present study (n = 10), the exact Mann–Kendall test was applied, as the sample size is less than 40. The significance of S was evaluated using critical values from Mann–Kendall tables for selected confidence levels. A positive S indicates an increasing trend, while a negative S indicates a decreasing trend.

For completeness, when a normal approximation was required for comparison, the variance of S was estimated as:

$$Var\,(S) = \frac{1}{18}\left[n\,(n-1)\,(2n+5) - \sum_{i=1}^{m} T_i(T_i - 1)(2T_i + 5)\right] \tag{6}$$

Here, m represents the number of tied groups in the time series, and t_i is the number of tied values within the i^{th} group.

The standardized statistic Z was computed as:

$$Z = \begin{cases} \frac{S-1}{\sqrt{Var(S)}} & if\; S > 0 \\ 0 & if\; S = 0 \\ \frac{S+1}{\sqrt{Var(S)}} & if\; S < 0 \end{cases} \tag{7}$$

To test the null hypothesis (H_0) of no trend, the absolute value of the test statistic |Z| is compared with the critical value $Z_{1-\alpha/2}$ from the standard normal distribution at selected significance levels α of 0.01, 0.05, 0.1. If |Z| > $Z_{1-\alpha/2}$, H_0 is rejected, indicating a significant trend at the 1- α

confidence level. A positive Z denotes an increasing trend, while a negative Z indicates a decreasing trend.

It is important to acknowledge that, during the near-term period (2015–2024), differences in radiative forcing among SSP scenarios are minimal (IPCC 2021; Chap. 4). The IPCC AR6 report shows that SSP-driven signals in climate variables remain largely indistinguishable during the first 10–15 years of projections. Scenario-specific trends only become statistically separable after approximately 2030, when the differences in cumulative emissions become more pronounced (IPCC 2021; O'Neill et al. 2016). Consequently, any divergence observed among SSP projections during 2015–2024 primarily reflects internal climate variability arising from natural atmospheric and oceanic fluctuations in the climate model, rather than differences in scenario-driven forcing. Therefore, the purpose of this near-term analysis is to evaluate the range of natural variability captured by the model ensemble, and to assess how well it reproduces observed short-term trends in Mediterranean wind patterns. The aim is not to identify which long-term emission pathway provides the most accurate projection. This assessment establishes a baseline for understanding model performance in simulating recent wind climate variability. This is essential for evaluating the reliability of mid- to long-term (post-2030) projections, where scenario-driven differences become statistically significant and physically meaningful.

Uncertainty assessment approach

Knowledge of the uncertainty related to wind climate models is considered highly important in assessing the uncertainty related to the projected changes in offshore wind energy. Hypothetically and statistically, if a model exhibits a bias relative to reference data during a historical period, it is plausible to assume that a similar bias will persist in future projections. Therefore, as both historical and future periods are influenced similarly, the model biases may not impact the projected change obtained using the same model. However, if the measured biases over the historical period present a significant range of uncertainty, this uncertainty will likely propagate into future projected climate, and the uncertainty related to the future projected changes may be amplified. The knowledge of the uncertainty associated with the computed model average and inter-averages bias uncertainty is also crucial for bias correction studies.

To quantify the relative differences between climate models and ERA5 reanalysis data, the normalized bias (NB) as a percentage is calculated as follows:

$$NB\,(\%) = \left(\frac{Model - ERA5}{ERA5}\right) x100 \tag{8}$$

where Model represents the climate model value and ERA5 represents the reanalysis value at the same location. Positive values indicate model overestimation, while negative values indicate underestimation relative to ERA5.

The uncertainty associated with the observed differences between ERA5 WS data and the evaluated climate model WS data, we employed the two-sample Student's t-test (independent samples t-test). This statistical test evaluates whether the observed differences between the two datasets are statistically significant and provides confidence intervals for these changes. The Student's t-test is a widely used parametric test (Decremer et al. 2014) and has been frequently applied in wind-wave climate change studies (Carrasco et al. 2014; Morim et al. 2019; Semedo et al. 2011). The null hypothesis of the t-test assumes no statistically significant difference between the means of the two samples, while the alternative hypothesis suggests a statistically significant difference at a given confidence level (1 − p-value). The p-values derived from the t-test represent the probability of obtaining a t-statistic less than the calculated value (t < t-test) under the null hypothesis. If the p-value is less than 0.05 (indicating a 95% confidence level), the null hypothesis is rejected. The t-statistic for the two-sample t-test is calculated as follows:

$$\boldsymbol{t} = \frac{\bar{\boldsymbol{x}}_2 - \bar{\boldsymbol{x}}_1}{\sqrt{\frac{\boldsymbol{S}_1^2}{\boldsymbol{n}_1} + \frac{\boldsymbol{S}_2^2}{\boldsymbol{n}_2}}} \tag{9}$$

$\bar{x}_1$ and $\bar{x}_2$ are the averages WS or WPD obtained from the climate models and reanalysis data successively, and S and n are their respective standard deviations and sample sizes.

In addition to the standard Student's t-test, Welch's t-test (Welch 1947) was employed to evaluate the statistical significance of the bias between the EC-Earth3 projections and the ERA5 reanalysis data. While the Student's t-test assumes equal variances between the samples being compared, Welch's t-test relaxes this assumption by adjusting the degrees of freedom using the Welch–Satterthwaite approximation (Ruxton 2006). This makes Welch's t-test more appropriate for comparing climate model outputs with reanalysis data, as these datasets may exhibit different levels of interannual variability. The test statistic is calculated using the same formula as in Eq. 9, but the degrees of freedom are estimated as follows:

$$\boldsymbol{df} = \frac{\left(\frac{\boldsymbol{S}_1^2}{\boldsymbol{n}_1} + \frac{\boldsymbol{S}_2^2}{\boldsymbol{n}_2}\right)^2}{\left[\frac{\left(\boldsymbol{S}_1^2/\boldsymbol{n}_1\right)^2}{(\boldsymbol{n}_1-1)} + \frac{\left(\boldsymbol{S}_2^2/\boldsymbol{n}_2\right)^2}{(\boldsymbol{n}_2-1)}\right]} \tag{10}$$

A 95% confidence level was applied to determine the statistically significant of the computed biases.

Estimating the confidence interval for the computed biases allows us to determine how precisely we can estimate the future projected change. The accurate estimation of the model biases allows a more accurate bias correction for historical and future data. The bias correction is a commonly used method in climate change studies (Dahunsi et al. 2025; Gohari and Akpinar 2024; Mohan and Bhaskaran 2019; Susini et al. 2022) to reduce the uncertainty related to model simulation accuracy. However, if the corrected bias is within a wide range of uncertainty, its correction will be more challenging. In most climate change studies and bias correction, the uncertainty related to the estimated bias is not considered. Furthermore, if the bias estimated for the historical period is characterized by low or insignificant uncertainty, the projection of future changes using the same models will be more accurate. Contrarily, if the estimated historical bias is high, the future projected changes may present higher uncertainty, which will add to the uncertainty related to the used scenario. Other error statistics such as RMSE, scatter index, and correlation were not used during the present study because the climate model, compared to hindcast models, does not present a correlation with reanalysis data. Climate models are based on historical and projected carbon emissions under different scenarios. Therefore, the models can only be evaluated based on the overall distribution considering different percentiles or based on the overall averages.

Results and discussion

Spatial accuracy of wind climate model simulations

The statistically significant differences measured in the wind speeds from 22 climate models simulations in comparison with the ERA5 wind speeds are presented in Fig. 2 for the whole Med Sea and summarized in Table 2 for the Med Sea sub basins. The significance of the change and the confidence intervals are computed using student t-test for a confidence level of 95% (Eq. 9). The sample size used for the Student's t-test is 30, corresponding to the annual average values of the compared models over a 30-year period. Considering that over the same sub-basin, both overestimated and underestimated biases can be observed (Fig. 2), and the averaged absolute biases are being considered for the spatial average bias over the sub-basins and the whole Med Sea in Table 2.

The maps presented in Fig. 2 show a remarkable discrepancy between the different models, in terms of normalized bias rate (Eq. 8), bias sign and bias significance. The results showed that most Med Sea regions' measured biases are statistically significant. The spatial distribution of the measured biases and their significance allow us to classify the models into eight groups. The first group includes five models (ACCESS-CM2, CMCC-ESM2, CMCC-CM2-SR5, CNRM-CM6-1 and HadGEM3-GC31-LL). The models of this first group show statistically significant underestimation of wind speed along the entire European coast and Algerian coast. On the other hand, an underestimation is also observed along the Tunisian coast and the southeastern Mediterranean coast. However, the normalized bias value is less pronounced in those regions. In the southern part of the Alboran basin, in the center of the Tyrrhenian basin, off the Libyan coast, off the Egyptian coast and off the Algerian coast, the model of the first group showed statistically significant overestimation the wind speed compared to ERA5. Among the models of this first group, the best-performing models are CMCC-CM2-SR5 and CNRM-CM6-1 models. The averaged absolute bias computed over the whole Mediterranean Sea for these two models is 0.69 m/s (Table 2). These models showed close performance at sub-basin scale as shown in Fig. 3.

The second group includes two models (AWI-CM-1-1-MR, and EC-Earth3). The normalized bias values computed for these two models are less important compared to the first group. Furthermore, the area with statistically significant bias at a confidence level of 95% is reduced. The second group showed, therefore, better performance across all Mediterranean regions. The models of the second group underestimate the wind speed along the French coast, the North Italian coast, the North Alboran Basin, the Eastern coast of Algeria and Tunisia, the western Mediterranean, and the northern part of the Aegean Sea. However, in the remaining coastal areas and in large offshore areas, the models are statistically significantly underestimating the wind speed. Among the two models of the 2nd group, the best-performing one is the EC-Earth3 model. The averaged absolute bias computed over the whole Med Sea for this model is 0.42 ± 0.10 m/s (Table 2). This value is the lowest among all the evaluated 22 models. Furthermore, EC-Earth3 model offers the lowest biases and confidence interval at most western and eastern Mediterranean sub-basins (Fig. 3).

The third group of models is composed of three different models (BCC-CSM2-MR, CNRM-CM6-1-HR and MRI-ESM2-0). Those models present a better spatial homogeneity over the Mediterranean in terms of bias values and sign. Among those models, the CNRM-CM6-1-HR showed the highest performance with a normalized bias $< 10\%$ over most the Mediterranean regions. Those models overestimate the ERA5 wind speed in a large part of the Mediterranean and underestimate it in the Aegean Sea and the Gulf of Lyon (French coasts). The fourth models group presented a large

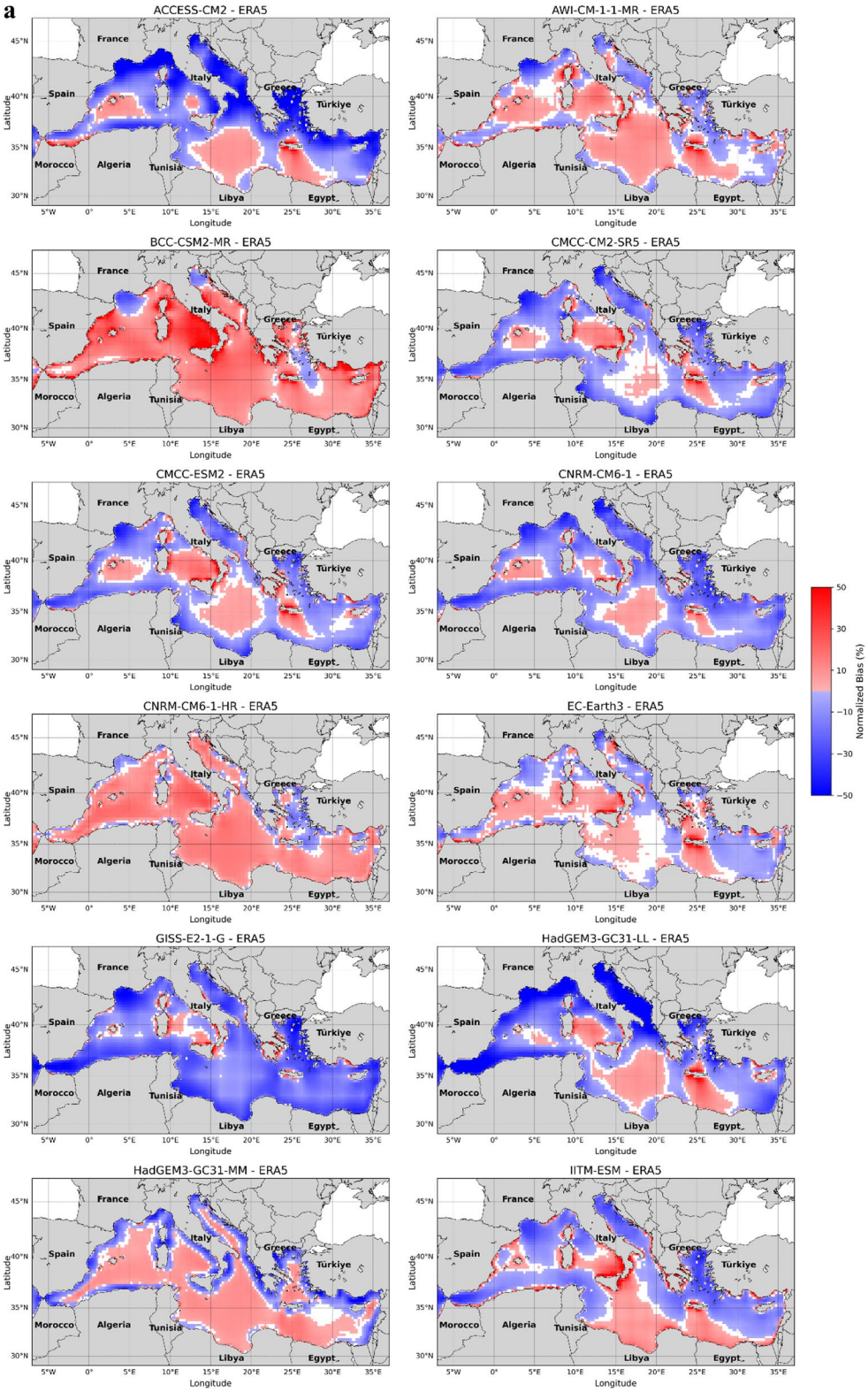


Fig. 2 **a** Bias graphs of each climate model against ERA5 wind speeds over the historical period 1985-2014. Red colors indicate overestimation, blue colors indicate underestimation, and white areas represent statistically non-significant biases ($p > 0.05$, Student's t-test). **b** Bias graphs of each climate model against ERA5 wind speeds over the historical period 1985-2014. Red colors indicate overestimation, blue colors indicate underestimation, and white areas represent statistically non-significant biases ($p > 0.05$, Student's t-test)

similarity in the spatial distribution of the normalized bias in wind speed compared to the third group. The models of this fourth group include MPI-ESM1-2 h, MPI-ESM-1–2-LR, MPI-ESM-1–2-HAM and NESM3. Contrarily to the third group models, those models showed higher underestimation over the French coast, in the north Aegean Sea, in the Adriatic Sea and at some Libyan and Egyptian coasts. Comparing bias results of the MPI-ESM1-2-HR high-resolution

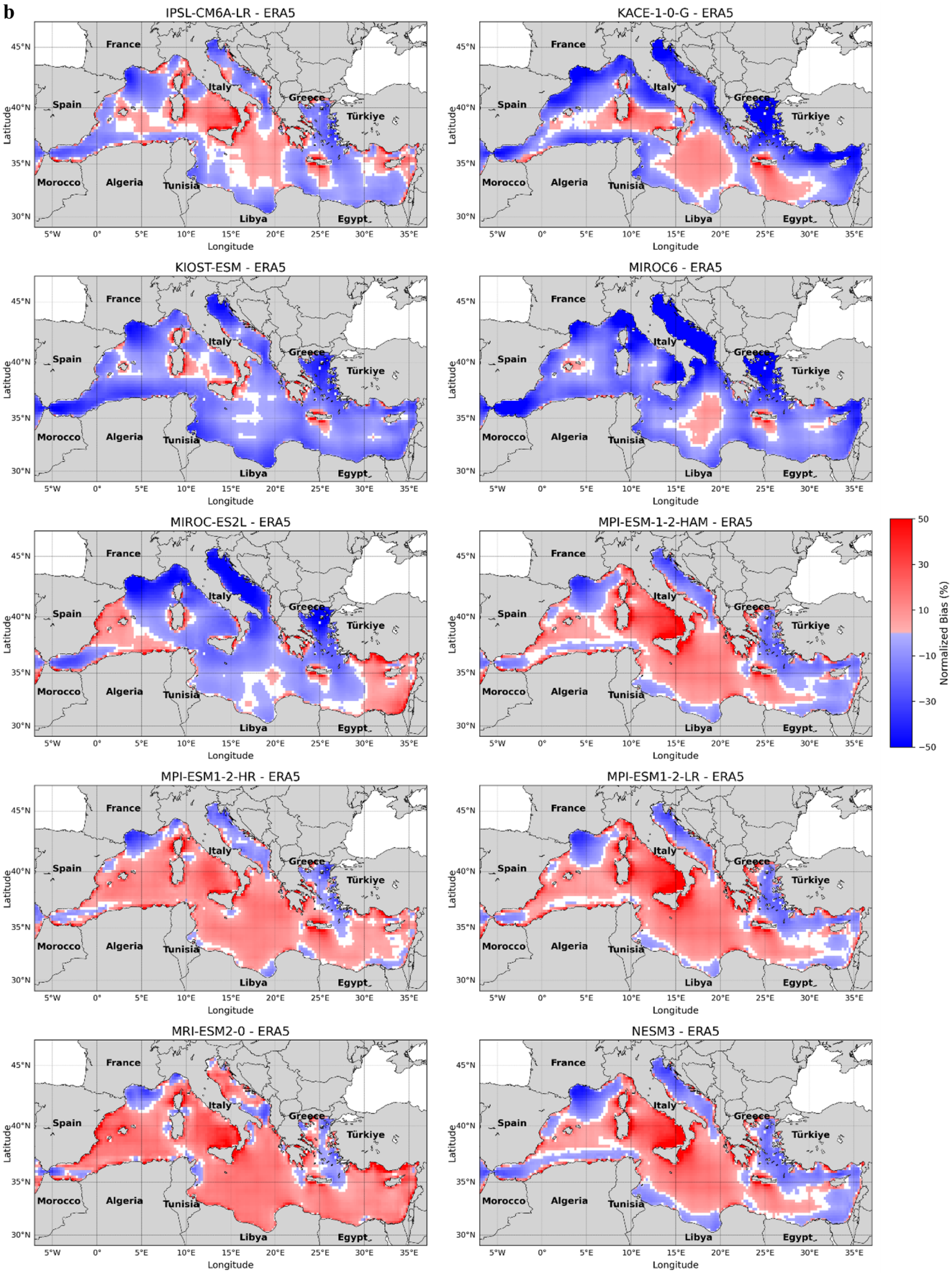


Fig. 2 (continued)

Table 2 Averaged absolute bias with confidence interval computed for 22 climate model over the 9 Mediterranean sub-basins and over the whole Med Sea for the historical period 1985–2014. Bold values indicate the model with the minimum bias for each sub-basin and for the entire Mediterranean Sea

	Alboran		Algerian		Balearic		Ligurian		Tyrrhenian	
	Bias	±CI	Bias	±CI	Bias	±CI	Bias	±CI	Bias	±CI
ACCESS-CM2	1.06	±0.11	1.08	±0.11	0.71	±0.09	2.42	±0.07	1.05	±0.10
AWI-CM-1-1-MR	**0.54**	**±0.11**	0.51	±0.13	**0.38**	**±0.10**	0.53	±0.09	0.52	±0.11
BCC-CSM2-MR	0.86	±0.12	0.89	±0.12	1.50	±0.11	0.76	±0.09	1.75	±0.13
CMCC-CM2-SR5	1.25	±0.09	0.77	±0.12	0.49	±0.10	0.52	±0.09	0.57	±0.12
CMCC-ESM2	1.27	±0.09	0.72	±0.11	0.49	±0.09	0.46	±0.09	0.65	±0.12
CNRM-CM6-1	1.44	±0.09	0.82	±0.11	0.45	±0.09	1.41	±0.08	0.5	±0.11
CNRM-CM6-1-HR	**0.46**	**±0.12**	0.63	±0.12	0.47	±0.11	**0.33**	**±0.10**	0.72	±0.11
EC-Earth3	0.58	±0.10	**0.35**	**±0.12**	**0.40**	**±0.10**	**0.33**	**±0.10**	**0.44**	**±0.11**
GISS-E2-1-G	2.25	±0.08	1.28	±0.10	0.45	±0.08	0.83	±0.08	0.44	±0.10
HadGEM3-GC31-LL	3.19	±0.08	1.33	±0.10	1.13	±0.08	2.28	±0.08	0.72	±0.10
HadGEM3-GC31-MM	0.74	±0.11	0.48	±0.13	0.48	±0.11	0.90	±0.09	0.49	±0.11
IITM-ESM	1.40	±0.09	0.67	±0.11	**0.36**	**±0.09**	0.75	±0.09	0.71	±0.11
IPSL-CM6A-LR	0.98	±0.10	0.59	±0.12	**0.38**	**±0.11**	0.52	±0.10	0.81	±0.11
KACE-1-0-G	1.42	±0.10	0.91	±0.12	1.12	±0.09	1.43	±0.08	0.9	±0.10
KIOST-ESM	1.99	±0.09	1.09	±0.10	0.48	±0.09	0.85	±0.08	**0.45**	**±0.09**
MIROC6	2.85	±0.08	1.06	±0.10	0.68	±0.08	2.62	±0.07	1.28	±0.09
MIROC-ES2L	1.19	±0.10	0.99	±0.11	0.68	±0.10	1.88	±0.08	0.81	±0.10
MPI-ESM1-2-HR	0.49	±0.11	0.71	±0.12	0.51	±0.10	0.51	±0.09	0.85	±0.11
MPI-ESM1-2-LR	0.63	±0.12	0.64	±0.13	0.48	±0.11	0.85	±0.10	1.6	±0.13
MPI-ESM-1–2-HAM	0.65	±0.12	0.59	±0.13	0.41	±0.10	0.67	±0.12	1.49	±0.14
MRI-ESM2-0	0.79	±0.10	0.75	±0.12	1.35	±0.11	0.71	±0.10	1.16	±0.11
NESM3	0.85	±0.12	0.64	±0.13	0.41	±0.10	0.60	±0.10	1.51	±0.13
	Eastern		Ionian		Aegean		Adriatic		Med Sea	
	Bias	±CI	Bias	±CI	Bias	±CI	Bias	±CI	Bias	±CI
ACCESS-CM2	0.62	±0.10	1.37	±0.10	2.23	±0.10	1.73	±0.07	1.36	±0.09
AWI-CM-1-1-MR	0.37	±0.11	0.52	±0.10	0.72	±0.12	0.52	±0.09	**0.51**	**±0.11**
BCC-CSM2-MR	0.73	±0.11	1.25	±0.12	0.87	±0.12	0.74	±0.1	1.04	±0.11
CMCC-CM2-SR5	0.48	±0.10	0.34	±0.11	0.94	±0.10	0.86	±0.08	0.69	±0.10
CMCC-ESM2	0.47	±0.10	**0.33**	**±0.11**	0.94	±0.11	0.88	±0.08	0.69	±0.10
CNRM-CM6-1	0.46	±0.10	0.57	±0.10	1.41	±0.10	1.12	±0.09	0.91	±0.10
CNRM-CM6-1-HR	0.57	±0.10	0.56	±0.10	**0.54**	**±0.12**	**0.40**	**±0.09**	**0.52**	**±0.11**
EC-Earth3	**0.27**	**±0.09**	**0.29**	**±0.09**	**0.61**	**±0.11**	**0.50**	**±0.09**	**0.42**	**±0.10**
GISS-E2-1-G	1.13	±0.09	0.87	±0.10	1.83	±0.11	1.04	±0.08	1.12	±0.09
HadGEM3-GC31-LL	0.48	±0.10	0.95	±0.09	1.19	±0.10	2.48	±0.07	1.53	±0.09
HadGEM3-GC31-MM	0.45	±0.10	0.73	±0.10	0.69	±0.11	0.53	±0.09	0.61	±0.11
IITM-ESM	0.49	±0.10	0.59	±0.12	1.39	±0.10	0.87	±0.08	0.81	±0.10
IPSL-CM6A-LR	0.39	±0.10	0.53	±0.10	0.99	±0.12	0.63	±0.09	0.65	±0.11
KACE-1-0-G	0.65	±0.10	0.68	±0.10	2.21	±0.10	1.57	±0.07	1.21	±0.10
KIOST-ESM	0.76	±0.09	0.52	±0.09	1.55	±0.10	1.06	±0.07	0.97	±0.09
MIROC6	0.66	±0.09	1.21	±0.09	2.23	±0.10	3.31	±0.06	1.77	±0.08
MIROC-ES2L	0.44	±0.09	0.89	±0.1	1.62	±0.10	2.07	±0.08	1.18	±0.10
MPI-ESM1-2-HR	0.46	±0.11	0.73	±0.11	0.82	±0.12	**0.49**	**±0.09**	0.62	±0.11
MPI-ESM1-2-LR	0.52	±0.12	1.06	±0.12	1.03	±0.12	0.69	±0.1	0.83	±0.12
MPI-ESM-1–2-HAM	0.48	±0.11	0.95	±0.12	1.03	±0.12	0.76	±0.09	0.78	±0.12
MRI-ESM2-0	0.76	±0.11	0.83	±0.11	0.65	±0.12	0.55	±0.09	0.84	±0.11
NESM3	0.52	±0.11	0.97	±0.12	0.93	±0.12	0.71	±0.09	0.79	±0.11

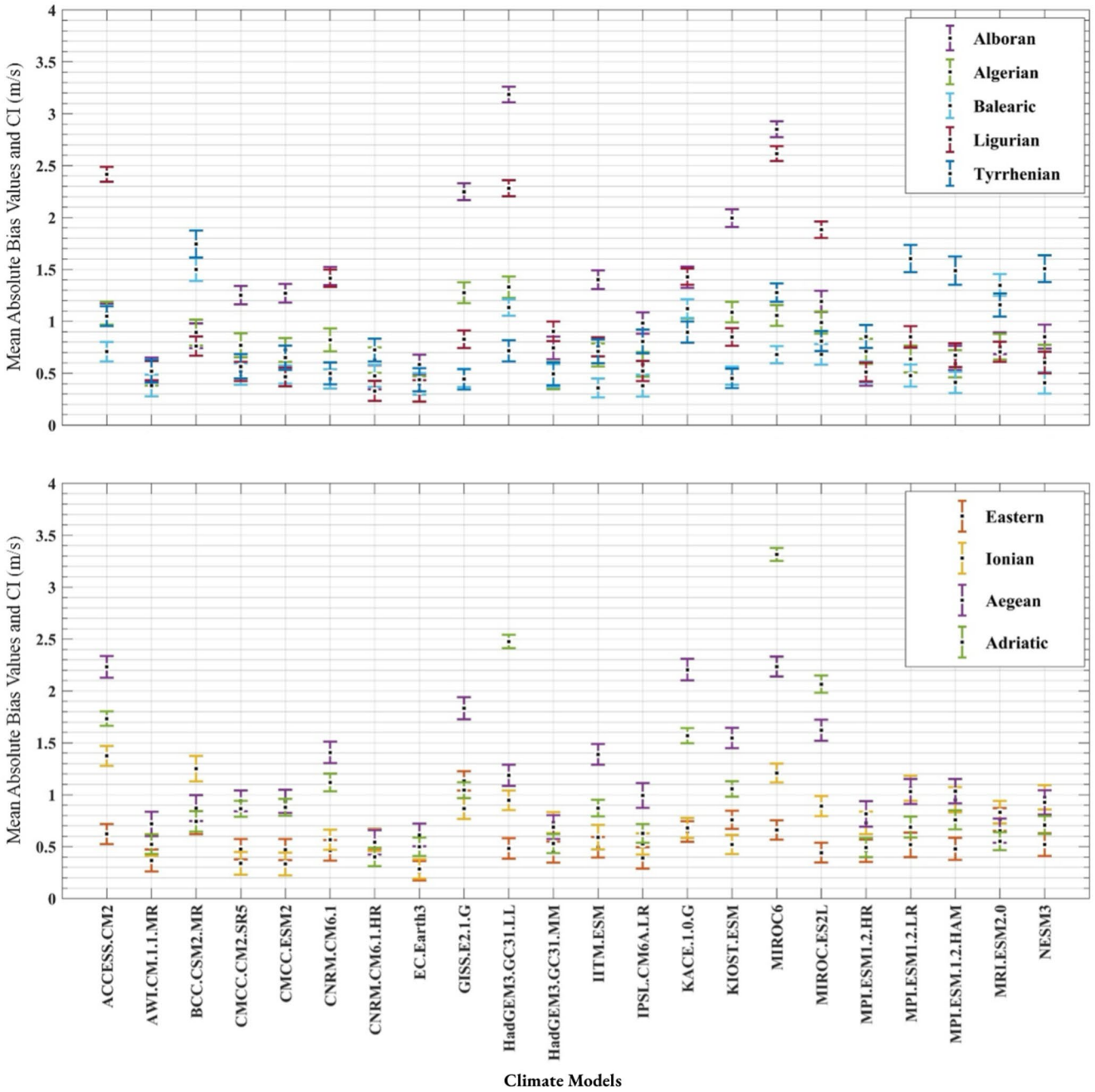


Fig. 3 Mean absolute bias values and 95% confidence intervals (CI) of wind speeds over the Mediterranean sub-basins from 22 climate models for the historical period 1985–2014

model against the MPI-ESM1-2-LR low-resolution model, we can notice that increase in model resolution may reduce the biases in some Mediterranean regions (e.g. the Tyrrhenian basin). However, the area with statistically significant change increased in the Algerian basin and the eastern Mediterranean Sea. Among the models of the 4th group, the best performing one is the MPI-ESM1-2-HR model. The averaged absolute bias computed over the whole Mediterranean Sea for this model is 0.62 ± 0.11 m/s (Table 2).

The fifth group, in terms of bias distribution, is composed of three models (GISS-E2-1-G, KIOST-ESM, and MIROC6). These models showed higher and statistically significant underestimation over a large part of the Med Sea. Therefore, these models are not recommended for any region considering that ERA5 is known to slightly underestimate wind speed compared to measurements (Çalışır et al. 2023). The 6th group, which is composed of three models (IITM-ESM, KACE-1-0-G and IPSL-CM6A-LR), also showed

statistically significant underestimation in most Mediterranean regions except in the southern part of the Tyrrhenian basin, off the Egyptian coast, around the Crete Island and off the Libyan coast. Among the models of the 6th group, IPSL-CM6A-LR is the most recommended, with an absolute bias average of 0.65 ± 0.11 m/s over the whole Mediterranean (Table 2). The two remaining models, HadGEM3-GC31-MM and MIROC-ES2L, showed different spatial distribution in the normalized biases compared to all previous models. The HadGEM3-GC31-MM model overestimates the wind speed in the offshore regions of the Mediterranean Sea and over the Egyptian and Libyan coasts and underestimates the wind speed over all remaining coastal regions. Furthermore, the bias values are low and homogenous in all offshore regions. This model can be highly recommended for offshore study and not recommended for coastal regions where statistically significant biases are observed. The average absolute bias computed for the HadGEM3-GC31-MM model is 0.61 ± 0.11 m/s over the whole Mediterranean Sea. Concerning the MIROC-ES2L model, the wind speeds are substantially underestimated in the Greek, French, Turkish and Italian regions and overestimated in the Balearic basin, off the Algerian coast and in the eastern Mediterranean basin. Therefore, this model is less recommended than previous models with one of the highest absolute bias values of 1.18 m/s ± 0.1 over the whole Med Sea (Table 2).

To better interpret the results presented in Table 2, the plot in Fig. 3 was created to observe the dispersion in the bias values and their confidence intervals computed for each model and over the Mediterranean sub-basins. The plot allows us to notice a large dispersion between the model results. Some models (e.g. KIOST-ESM, MICRO-ES2L, GISSE2-1G and NESM3) present a good accuracy in some sub-basins but a bad accuracy in others. This kind of model may not be recommended for the Mediterranean scale climate change studies. On the other hand, some models like CNRM.CM6-1-HR, EC-Earth3, HadGEM3-GC31-MM, and AWI-CM-1-1-MR showed good and close performance in the overall sub-basins. Regarding the confidence interval in the estimated biases, we can notice that at some sub-basing and even if the models present a high absolute bias, the confidence interval range can be low. A low confidence interval reflects a better statistical fitting to ERA5 data in terms of distribution and may allow a better result after a statistical bias correction for the model results. The models presenting at the lower biases and lower confidence interval range over most sub-basins are: CNRM-CM6-1-HR, EC-Earth3, HadGEM3-GC31-MM, AWI-CM-1-1-MR and MPI-ESM1-2-HR.

Based on the results presented in Table 2; Fig. 3, the best models recommended for each sub-basing are mapped in Fig. 4. The results showed that the EC-Earth3 model is the most recommended among all models for a large part of the Mediterranean Sea. EC-Earth3 showed the best performance in the Algerian basin, the Eastern Mediterranean basin, and the Ionian basin and is also recommended for the Balearics, the Tyrrhenian, the Ligurian, the Adriatic, and the Aegean basins. In the Alboran basin, the most recommended models are CNRM-CM6-1-HR and the MPI-ESM1-2-HR. However, based on the results presented in Fig. 3, EC-Earth3 model presented a low bias value of 0.58 ± 0.10 m/s at this region. Furthermore, as an alternative model to EC-Earth3 at Mediterranean scale, CNRM-CM6-1-HR which is more recommended for the Albertan Basin, also present a good accuracy over the whole Mediterranean basin and can also be recommended for Adriatic, Ligurian, and Aegean basins



Fig. 4 The most suggested wind climate models per Mediterranean sub-basins according to bias analysis results with respect to ERA5 reanalysis data

(Fig. 4). Therefore, we highly recommend both EC-Earth3 and CNRM-CM6-1-HR for wind speed and wind energy climate changes study for the Mediterranean Sea.

The spatial comparison of CMIP6 models with ERA5 reveals statistically significant inter-model variability across Mediterranean sub-basins. While previous studies (Carvalho et al. 2021; Martinez and Iglesias 2023) evaluated CMIP6 multi-model ensembles for Europe and the Mediterranean, our model-by-model assessment demonstrates that individual model performance varies considerably by region. EC-Earth3 showed the best overall performance with the lowest averaged absolute bias (0.42 ± 0.10 m/s) across the Mediterranean, consistent with its reported accuracy in European wind climate studies (Carvalho et al. 2021). In contrast, models such as BCC-CSM2-MR, which was included in previous Mediterranean ensemble studies (Carvalho et al. 2021), exhibited substantially larger biases (1.04 ± 0.11 m/s) more than double that of EC-Earth3 highlighting the risk of relying on ensemble means that may mask such regional errors. Unlike ensemble-based approaches that implicitly assume equal model contributions (e.g., Akinsanola et al. 2021; Claro et al. 2023), our sub-domain-specific evaluation provides transparent guidance for model selection in regional wind resource assessments and emphasizes the need for performance-based model weighting in future Mediterranean wind climate projections.

Model performance in estimating WPD

To deeper assess the performance of the best models (EC-Earth3 and CNRM-CM6-1-HR) recommended in terms of the spatial measured wind speed biases and to assess the model accuracy in estimating wind power density and their related uncertainties. Both models' WS and WPD estimates are compared to ERA5-based estimations at 12 reference locations (Fig. 1). Knowing that the WPD is computed as a third-degree power of WS, the errors related to the wind speed estimates and the confidence interval of the estimated averages may be amplified. Therefore, to study the impact of climate change in wind energy resources the models' uncertainty in terms of wind speed will not be sufficient to determine their uncertainty in estimating and projecting wind power changes. Furthermore, as long as the model performance may change as a function of the estimated wind speed, and some models used to overestimate the lower wind speed and underestimated extreme wind speed, the models' accuracy was evaluated based on the data distribution by comparing the estimated percentile values and not only based on the total averages.

The normalized differences of the CNRM-CM6-1-HR model relative to ERA5 WS and WPD percentile values are presented in Fig. 5. In the graphs, the continuous line shows the difference of the model's WS percentile values with respect to ERA5 WS, and the dashed line shows the difference of the model's WPD percentile values with respect to ERA5-based WPD. Shaded areas indicate the confidence interval for the estimated differences between the models and ERA5 percentile values estimated using the two-sample t-test. The shaded areas reflect the confidence, and the uncertainty related to the estimated biases. A low confidence interval indicates a good fit between the compared data and, therefore, more possibility to perform an accurate bias correction using statistical methods to improve the projection results. The red represents the model's overestimation compared to ERA5, while the blue represents the model's underestimation. The dark-shaded areas indicate the confidence intervals at the 5% significance level of the difference of the model percentile values for WS, and the light-shaded areas indicate the difference of the model percentile values for WPD against ERA5 percentile values.

The assessment of the model performance in estimating the lower and higher WS and WPD allows us to better evaluate the model projection uncertainty, which may be related to the projected changes in wind speed distribution. For instance, a model with poor accuracy in estimating extreme wind speed can project higher uncertainty if the extreme events increase in favor of normal events in the future. This type of uncertainty may not be evaluated based on the averaged values. Therefore, the model accuracy should be evaluated over all the distribution ranges. This method was previously applied by Çakmak et al. (2025) to assess the model's performance in estimating wave storm events in the Black Sea.

As can be seen in Fig. 5, the CNRM-CM6-1-HR model overestimates the percentile values of WS and WPD in the western part of the Mediterranean Sea (ST.1 to ST.6) compared to ERA5 at all percentiles except for ST.1 and ST.2, where the model showed a good accuracy for the first 10 percentiles. Even with the observed overestimations, at ST.1, CNRM-CM6-1-HR shows good agreement with ERA5 for most of the percentiles with normalized bias values between 0.05 and 0.1 for WS and between 0 and 0.4 for WPD. The location where the model is least in agreement with ERA5 is ST.6 in the Tyrrhenian Basin. CNRM-CM6-1-HR WPD normalized differences reached 1.6 at that station, which reflects the high uncertainty that may result from model accuracy in climate change studies and the highest dependence of the model accuracy to the study location.

In the eastern parts of the Mediterranean, the CNRM-CM6-1-HR model underestimates both WS and WPD in the Aegean Basin (ST.11) below the 90th percentile and in the Eastern Mediterranean Basin (ST.12) below the 50th percentile. In the central region of the Eastern Mediterranean Basin (ST.10), the model underestimates WS and WPD

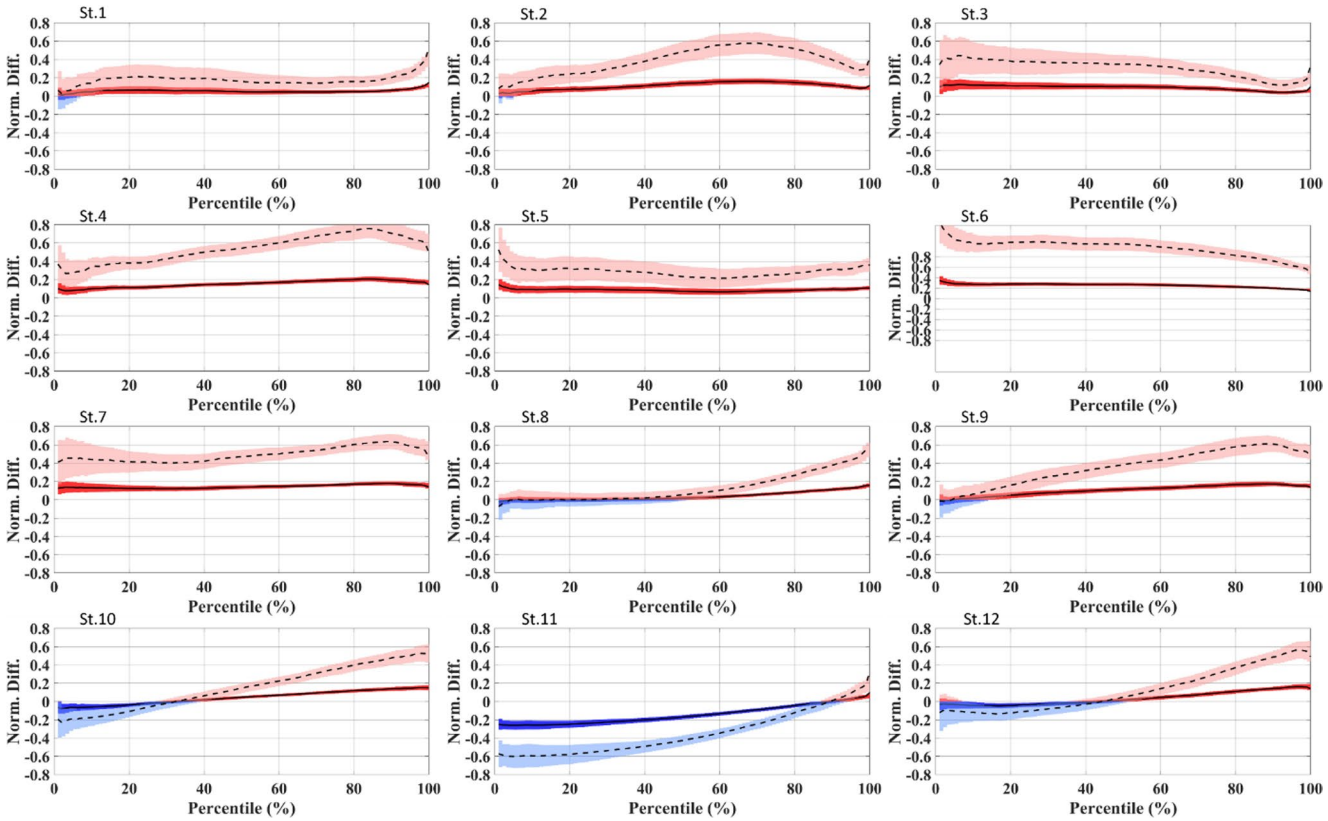


Fig. 5 Normalized differences per percentile values of WS (Solid line) and WPD (Dashed line) derived from CNRM-CM6-1-HR climate model against ERA5 over the historical period 1985–2014 with the associated confidence interval. The red color reflects overestimated percentiles, and the blue color showed the underestimated percentiles

below the 30th percentile, while at higher percentiles, the model overestimates ERA5 for both WS (up to 0.2) and WPD (up to 0.6). In the Adriatic Sea (ST.8), the model gives very low differences (lower than 0.05) compared to ERA5 below the 60th percentile of WS and the 50th percentile of WPD. In this region, the overestimation of the model is observed at the higher percentiles of WS and WPD. In the Ionian Basin (ST.9), similar to ST.1 and ST.2 locations in the western region, the model underestimates the below 10th percentile, especially for confidence intervals.

In summary, the CNRM-CM6-1-HR model-derived WPD showed a statistically significant overestimation exceeding 50% for most percentiles, especially for the highest percentile values. The model accuracy in estimating the WPD percentiles changes considerably as a function of the location. The best results obtained for CNRM-CM6-1-HR were observed at ST.1 in the Alboran Basin and in the Adriatic Basin; however, at those two locations, the model presents substantial overestimation of the higher percentiles. Regarding the model uncertainty in the estimated differences, the confidence interval ranges are predominantly larger for the lower percentile and exceeded 40% at several locations, such as ST.3, ST.5, and ST.7.

Figure 6 shows the normalized differences of the EC-Earth3 model compared to ERA5 values for WS and WPD percentiles. EC-Earth3 overestimates WS and WPD in all percentiles at ST.4 and ST.6 locations in the western Mediterranean, similar to the CNRM-CM6-1-HR model but with lower and more stable normalized differences overall percentiles. At the remaining four locations in the western region (ST.1, ST.2, ST.3, ST.5), in contrast to CNRM-CM6-1-HR, slight underestimations at high percentiles can be noticed. In the Algerian Basin (ST.3 and ST.4), the differences of EC-Earth3 against ERA5 WS and WPD percentile values are less than 0.2. At ST.3, the model slightly underestimates WS and WPD compared to ERA5 in almost all percentiles. In the western Mediterranean, the highest differences are again seen at ST.6, but the differences are slightly lower than in the CNRM-CM6-1-HR model, 0.2 and 0.8 for WS and WPD, respectively.

In the eastern part of the Mediterranean, EC-Earth3 underestimates both WS and WPD compared to ERA5, covering a wider range of percentiles than that of CNRM-CM6-1-HR at all locations except ST.7 and ST.11. In these four locations, EC-Earth3 overestimates the 90th percentile values between 0 and 0.05 differences for WS and between

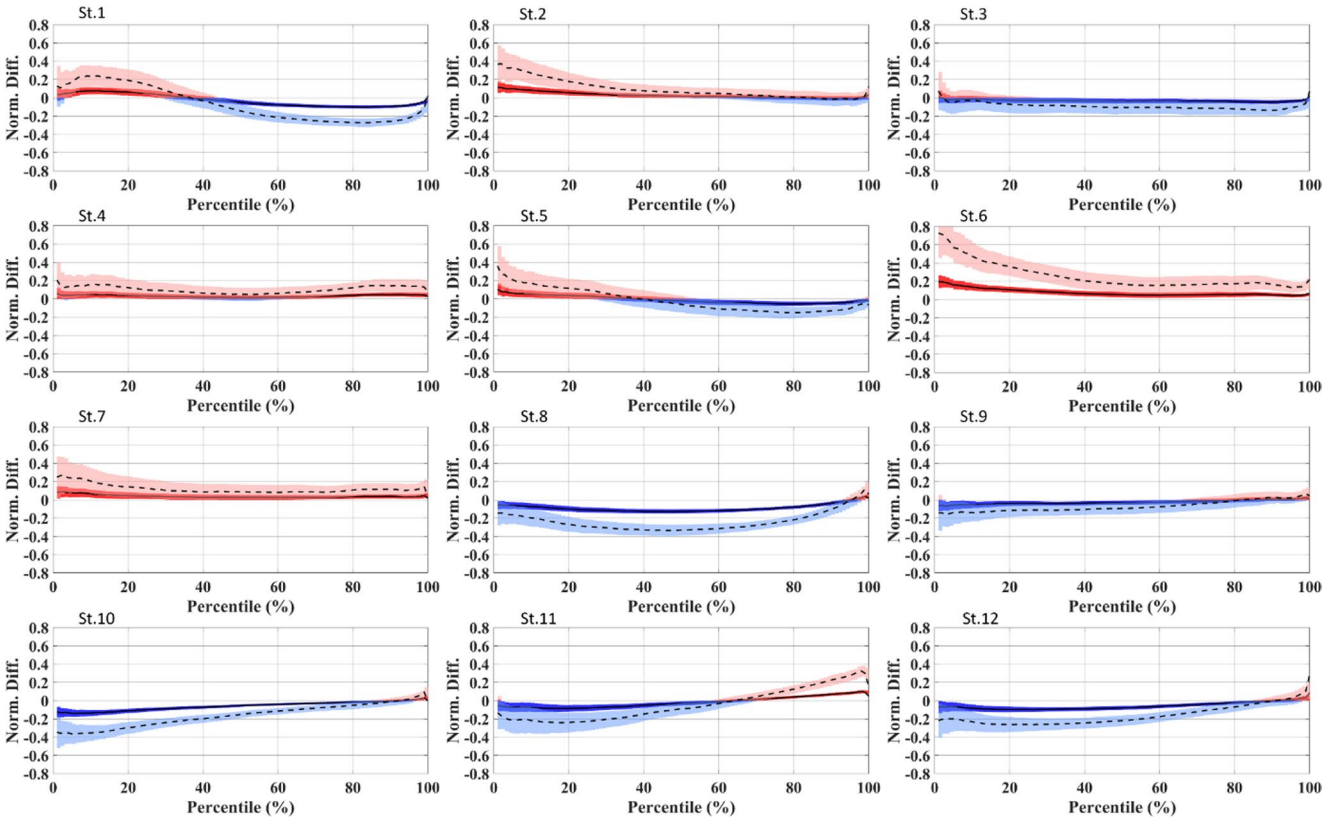


Fig. 6 Normalized differences per percentile values of WS (Solid line) and WPD (Dashed line) derived from EC-EARTH3 climate model against ERA5 over the historical period 1985–2014 with the associated confidence interval. The red color reflects overestimated percentiles, and the blue color showed the underestimated percentiles

0 and 0.2 differences for WPD. At the Aegean Basin (ST.11), an overestimation for the values above the 70th percentile is observed using the EC-Earth3 model. Above the 90th percentile, EC-Earth3 slightly overestimates the WPD compared to CNRM-CM6-1-HR at ST.11 (Aegean Basin); however, at all remaining percentiles, EC-Earth3 is more in agreement with ERA5. Therefore, EC-Earth3 is more recommended in the Aegean Basin. This finding was not reached considering the average-based biases (Table 2), where the EC-Earth3 absolute bias in the Aegean Basin was higher than the CNRM-CM6-1-HR absolute bias.

Over the Mediterranean Sea, EC-Earth3 shows lower differences compared to ERA5 percentile values for WS and WPD. In general, CNRM-CM6-1-HR is used to overestimate the WS and WPD, whereas EC-Earth3 has a more balanced performance. Especially for extreme values (above 90th percentile), EC-Earth3 has much lower differences (±0.2) with ERA5, except in the Aegean Basin ST.11. Regarding the confidence interval ranges, the EC-Earth3 model shows a better performance at most locations. In both models, the confidence interval ranges of low percentile values are higher than those of high percentile values.

Our percentile-based WPD evaluation extends beyond the mean-value approaches used in previous Mediterranean studies (Carvalho et al. 2021; Claro et al. 2023; Lira-Loarca et al. 2021). By examining the full WPD distribution (5th to 95th percentiles), we demonstrate that model accuracy varies substantially between typical and extreme wind events. EC-Earth3 maintained consistent performance across all percentiles with normalized differences generally within ±0.2, while CNRM-CM6-1-HR systematically overestimated high percentiles, particularly in the Tyrrhenian Basin (ST.6) where WPD normalized differences reached 1.6 at the 95th percentile. This is critical for wind energy planning, as relying solely on mean values can mask biases in extreme events that affect wind farm design, capacity factor estimates, and risk assessment. Our approach provides a more robust framework for evaluating model reliability compared to ensemble-mean methods commonly applied in previous CMIP6 assessments. Furthermore, the percentile-based evaluation revealed that EC-Earth3 outperforms CNRM-CM6-1-HR in the Aegean Basin a finding not evident from average-based bias analysis (Table 2) demonstrating the added value of distributional assessment for regional model selection.

Assessment of near-term projected wind climate change

In this section, the ERA5 reanalysis dataset is compared with the EC-Earth3 climate model under different SSP scenarios, and the consistency between these datasets is assessed at selected reference points in terms of wind speed (WS) and wind power density (WPD). Figure 7 presents the trends of WS projections based on ERA5 data at 12 reference stations and different future simulations of EC-Earth3 for the period 2015–2024. As discussed in Sect. 3.2, the differences in radiative forcing between SSP scenarios over this 10-year period are minimal (IPCC 2021). Therefore, the divergence observed among SSP projections primarily reflects internal climate variability within the models rather than differences in scenario-driven forcing. The following analysis evaluates how well the EC-Earth3 ensemble captures observed short-term trends and the range of natural variability in Mediterranean wind patterns.

Table 3 shows the significant biases and uncertainties of EC-Earth3 future simulations compared to ERA5 WS and WPD for the 2015–2024 period. A 95% confidence interval was used for the Welch t-test (Eqs. 9–10) to measure the significance of the bias. Bolded values indicate significant biases for scenarios compared to ERA5. The uncertainty interval (CI) is given by ± for each scenario, along with the bias values relative to ERA5. A narrow CI range, typically ± 0.15–0.25 m/s, indicates statistically reliable differences between EC-Earth3 and ERA5 based on ten years of data referring the significance test results with a confidence interval of 95%. Across the Mediterranean, the EC-Earth3 model reproduces the near-term mean wind speed climatology (2015–2024) with generally small deviations from ERA5, typically within ± 0.5 m/s. These differences are within the expected range for coarse-resolution GCM outputs, indicating that the model reasonably well captures the large-scale atmospheric circulation that influences Mediterranean wind patterns across all SSP scenarios.

Slight underestimations are found over the Alboran (ST.1) and Ligurian (ST.5) basins (≈ − 0.3 to − 0.4 m/s) consistent with the model's limited ability to represent strong zonal flow and topographically accelerated winds through the Strait of Gibraltar and along the Ligurian coast. Conversely, the Balearic basin (ST.2) shows a weak positive bias, suggesting that the model slightly overestimates open-sea winds in this less-orographically constrained area. The northern and southern locations of the Algerian basin (ST.3 and ST.4) exhibits contrasting behavior, with an underestimation in the north and near-neutral or slightly positive bias farther south. The Tyrrhenian basin (ST.6) and Tunisian shelf (ST.7) show modest positive biases (up to + 0.36 m/s),

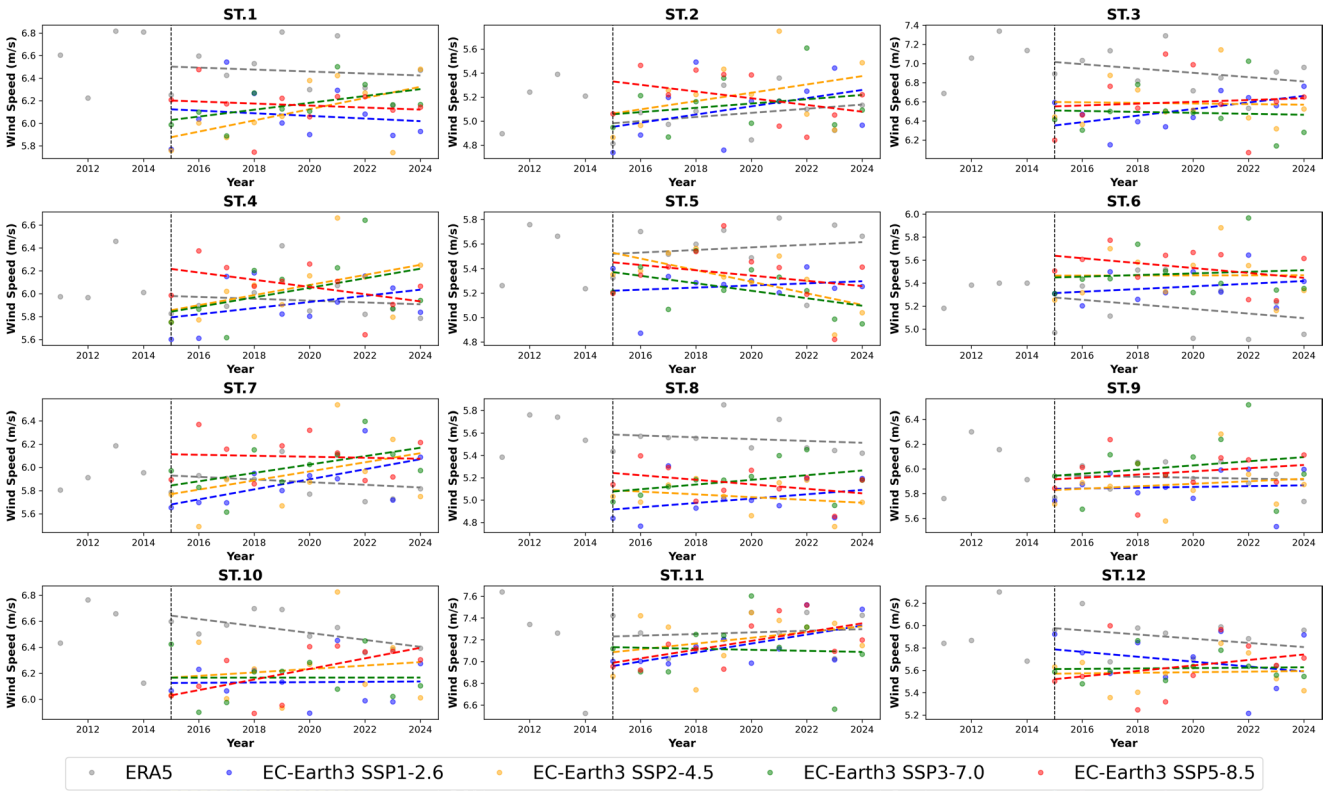


Fig. 7 Near term (2015–2024) divergence between ERA5 and EC-Earth3 future scenarios for annual mean wind speeds

Table 3 The differences and uncertainties between WS and WPD derived from EC-Earth3 scenarios and ERA5 over the near-term period 2015–2024. The values in red colors show the significant biases using Weltch's t-test at 95% confidence

WS Bias ± CI (m/s)				
Locations	**SSP1-2.6**	**SSP2-4.5**	**SSP3-7.0**	**SSP5-8.5**
ST.1	**-0.39 ± 0.21**	**-0.36 ± 0.23**	**-0.30 ± 0.19**	**-0.30 ± 0.19**
ST.2	0.05 ± 0.21	0.16 ± 0.22	0.08 ± 0.19	0.14 ± 0.18
ST.3	**-0.41 ± 0.19**	**-0.33 ± 0.22**	**-0.43 ± 0.22**	**-0.32 ± 0.25**
ST.4	-0.03 ± 0.19	0.11 ± 0.22	0.09 ± 0.23	0.13 ± 0.18
ST.5	**-0.31 ± 0.18**	**-0.25 ± 0.21**	**-0.33 ± 0.19**	-0.21 ± 0.22
ST.6	0.18 ± 0.19	**0.28 ± 0.22**	**0.30 ± 0.21**	**0.36 ± 0.20**
ST.7	-0.00 ± 0.17	0.07 ± 0.24	0.13 ± 0.17	**0.22 ± 0.16**
ST.8	**-0.55 ± 0.15**	**-0.52 ± 0.13**	**-0.38 ± 0.14**	**-0.40 ± 0.14**
ST.9	-0.08 ± 0.13	-0.06 ± 0.15	0.09 ± 0.19	0.04 ± 0.14
ST.10	**-0.39 ± 0.14**	**-0.30 ± 0.20**	**-0.36 ± 0.15**	**-0.31 ± 0.16**
ST.11	-0.12 ± 0.18	-0.06 ± 0.20	-0.15 ± 0.22	-0.09 ± 0.18
ST.12	**-0.20 ± 0.20**	**-0.31 ± 0.16**	**-0.27 ± 0.14**	**-0.26 ± 0.20**
WPD Bias ± CI (W/m²)				
Locations	**SSP1-2.6**	**SSP2-4.5**	**SSP3-7.0**	**SSP5-8.5**
ST.1	**-200.84 ± 63.08**	**-182.83 ± 80.23**	**-163.55 ± 65.15**	**-165.25 ± 63.16**
ST.2	-21.95 ± 51.50	12.41 ± 62.90	-26.94 ± 55.06	13.91 ± 29.91
ST.3	**-189.65 ± 96.35**	**-152.86 ± 115.42**	**-210.60 ± 112.67**	**-167.16 ± 124.47**
ST.4	-34.49 ± 67.52	58.07 ± 88.48	18.17 ± 94.18	49.87 ± 65.65
ST.5	**-123.73 ± 60.23**	**-100.87 ± 60.44**	**-141.46 ± 57.25**	**-104.43 ± 65.61**
ST.6	4.83 ± 47.42	**69.87 ± 53.43**	46.24 ± 67.48	**65.37 ± 54.97**
ST.7	-8.72 ± 50.50	30.96 ± 76.53	23.64 ± 66.49	**50.63 ± 50.17**
ST.8	**-111.17 ± 36.45**	**-95.38 ± 35.39**	**-62.46 ± 39.81**	**-77.03 ± 35.86**
ST.9	-29.84 ± 48.59	-10.74 ± 58.51	15.06 ± 67.02	14.85 ± 47.24
ST.10	**-79.50 ± 50.24**	-39.93 ± 70.63	**-72.87 ± 54.54**	-50.71 ± 52.72
ST.11	46.16 ± 68.10	**84.71 ± 77.17**	38.63 ± 93.88	73.38 ± 85.79
ST.12	-16.27 ± 45.04	-32.94 ± 45.93	**-47.32 ± 39.99**	-22.70 ± 58.82

which may stem from a smoother representation of coastal roughness and enhanced mixing over open water.

The largest negative bias (≈−0.5 m/s) is found in Adriatic (ST.8) under all scenarios, likely due to the model's inability to resolve strong mesoscale winds that dominate this semi-enclosed basin. In the Ionian (ST.9) and Aegean (ST.11) basins, biases are small (−0.15 to +0.1 m/s), while the central (ST.10) and far eastern Mediterranean (ST.12) show mild underestimations (≈−0.3 m/s). These regions are generally characterized by weaker synoptic forcing and more homogeneous open-sea conditions, which the model reproduces more consistently.

Across all 12 locations, differences among the four SSP scenarios are minimal, typically less than 0.2 m/s. This confirms that, in the near-term period, variations in external forcing among SSP1-2.6, SSP2-4.5, SSP3-7.0, and SSP5-8.5 exert negligible influence on mean wind speed. These findings are consistent with the IPCC AR6 (WGI, Chap. 4), which shows that scenario-specific forcing differences remain small before mid-century. Any minor trend toward reduced underestimation in higher-forcing scenarios (e.g., SSP5-8.5) is not statistically significant and likely reflects internal variability rather than a physical response to scenario forcing.

According to the Welch t-test results, only a subset of the biases (at locations ST.1, ST.3, ST.8, ST.10, and ST.12) are statistically significant at the 95% confidence level, primarily those with larger deviations (ranging from −0.20 to 0.55 m/s) from ERA5. At most other locations, biases are statistically non-significant, indicating that EC-Earth3 reproduces the observed near-term mean wind speed realistically across most of the basin, however this uncertainty in the estimated average value should be considered in future climate change projection.

Compared to wind speed, the WPD biases show similar spatial patterns but with larger magnitudes and variability. Even small wind speed deviations thus result in amplified WPD differences, consistent with the cubic dependence

of WPD on wind speed. The largest underestimations (up to −200 W/m²) occur in the Alboran (ST.1), north of the Algerian (ST.3), and Adriatic (ST.8) basins, reflecting the model's limited ability to capture mesoscale wind systems. In contrast, positive biases over the Tyrrhenian and Tunisian shelf regions (≈+50–70 W/m²) indicate a tendency toward overestimation in open-sea or smoother-terrain environments. Among scenarios at the same location, WPD differences remain small (< 80 W/m²) and lack a systematic trend, confirming that near-term scenario forcing has little impact on regional wind energy potential. Statistically significant deviations are limited to locations with the largest negative biases, while most remain non-significant, suggesting that EC-Earth3 generally reproduces the Mediterranean wind power climatology realistically, albeit with biases amplified relative to mean wind speed.

Table 4 shows the Theil-Sen slopes (Eq. 3) for WS and WPD based on the ERA5 reanalysis and EC-Earth3 scenarios, along with their statistical significance evaluated through the Mann-Kendall test (Eqs. 4–7). In the near-term period (2015–2024), both ERA5 reanalysis and EC-Earth3 simulations reveal low trends in average wind speed across the Mediterranean. Most trends fall within the range of ±0.05 m/s/year and this indicates that large-scale patterns have remained relatively stable, consistent with the short 10-year timescale and internal climate variability dominating over forced responses. ERA5 primarily shows neutral to slightly negative trends, while EC-Earth3 SSPs showed a mixture of positive and negative trends depending on location and scenario. Statistically significant positive trends were only detected for ST.1, ST.4, and ST.7 under specific scenarios (SSP2-4.5 and SSP1-2.6), implying localized projected increase in winds speed in these regions. However, no significant increasing trend was not observed based on ERA5 data. Given the short evaluation period and considering the fact that ERA5 represents the actual climate system, and that CMIP6 simulation represents a no deterministic forecast, the observed significant increases can be interpreted as expressions of internal variability rather than evidence of externally forced change.

At the remaining locations and SSPs non-significant increase or decrease was observed. The no systematic increase or decrease was observed across SSPs, confirming that short-term changes in external forcing have minimal impact on the evolution of average wind speeds.

Table 4 Theil-Sen trend slopes and their significance according to the Mann-Kendall test computed for the WS and WPD derived from ERA5 data and EC-Earth3 scenarios over the near-term period 2015–2024. The values in red colors show the slope with significant trend

WS Trend Slope (m/s/year)					
Locations	**ERA5**	**SSP1-2.6**	**SSP2-4.5**	**SSP3-7.0**	**SSP5-8.5**
ST.1	-0.012	-0.014	**0.073**	0.020	-0.007
ST.2	0.017	0.042	0.044	0.016	-0.028
ST.3	-0.017	0.036	-0.002	-0.015	0.020
ST.4	-0.005	0.032	**0.045**	0.049	-0.030
ST.5	0.021	-0.009	-0.043	-0.039	-0.001
ST.6	-0.010	0.020	0.002	0.004	-0.013
ST.7	-0.014	**0.048**	0.046	0.030	-0.001
ST.8	-0.017	0.032	-0.006	0.045	-0.018
ST.9	0.001	0.007	0.011	0.031	0.013
ST.10	-0.024	-0.005	0.012	0.008	0.035
ST.11	0.004	0.045	0.007	0.002	0.054
ST.12	-0.011	-0.023	0.002	0.002	0.030
WPD Trend Slope (W/m²/year)					
Locations	**ERA5**	**SSP1-2.6**	**SSP2-4.5**	**SSP3-7.0**	**SSP5-8.5**
ST.1	-7.26	**-5.33**	16.19	10.73	-1.79
ST.2	1.44	13.65	10.23	0.78	-0.39
ST.3	-13.5	10.56	3.24	-1.58	23.09
ST.4	-3.41	7.59	10.05	22.72	-5.27
ST.5	3.02	-2.63	**-11.03**	0.8	-1.88
ST.6	-1.76	5.06	-1.29	0.92	5.94
ST.7	-3.45	15.65	12.76	**16.58**	2.58
ST.8	-0.79	5.3	-2.1	6.95	-1.62
ST.9	-4.46	5.67	5.49	10.92	7.62
ST.10	-6.16	4.14	5.18	-1.75	11.88
ST.11	0.09	9.3	11.19	4.52	15.63
ST.12	-6.98	**-2.38**	3.49	3.14	8.95

Wind power density (WPD) trends exhibit similar spatial patterns but with high magnitude and variability. ERA5 indicates mostly weak or negative trends, consistent with slightly declining near-surface winds. EC-EARTH3 results show alternating positive and negative slopes (within ±15 W/m^2/yr), with notable positive trends (≈+10–25 W/m²/year) at several locations (ST.3, ST.4, ST.7, ST.11). Among these, ST.5 (SSP2-4.5) and ST.7 (SSP3-7.0) exhibit statistically significant changes, suggesting potential regional wind energy enhancement signals. Overall, EC-Earth3 realistically reproduces the weak and heterogeneous near-term wind speed and wind power density trends observed in ERA5, without containing a clear signal dependent on the scenario. The limited duration of the evaluation period (2015–2024) constrains the ability to robustly identify which SSP scenario provides the best representation of the present climate. Over such a short timescale, internal climate variability can dominate over externally forced differences, reducing the reliability of scenario discrimination.

Figure 8 illustrates the trends of WPD projections calculated based on different future simulations of ERA5 and EC-Earth3 at reference stations for the period 2015–2024. It is important to note that the WPD values presented here represent the theoretical kinetic energy available in the wind at 90 m hub height, rather than actual electricity generation potential. According to the Betz limit, a maximum of approximately 59.3% of the wind's kinetic energy can theoretically be converted to electricity by an ideal wind turbine (Betz 1926; Manwell et al. 2009). In practice, modern offshore wind turbines typically achieve capacity factors of 35–45% due to additional losses from mechanical efficiency, electrical conversion, wake effects, and operational constraints (IRENA 2023; Staffell and Pfenninger 2016), meaning actual energy production would be approximately 30–40% of the theoretical WPD values presented. Additionally, the offshore wind industry is moving towards taller turbines (120–150 m hub heights), which would experience 5–8% higher wind speeds than our 90 m estimates due to vertical wind shear, following the power-law wind profile with a typical offshore shear exponent of 0.11 (IEC 61400-1, 2019). Practical deployment in the Mediterranean also faces spatial constraints, as turbines are typically installed within ~30 km from shore and at water depths up to ~1 km, though floating technologies are enabling access to deeper waters (IRENA 2023). The WPD derived from ERA5 winds exhibited a decreasing trend at all stations except ST.2. At ST.1, the most closely aligned with the decreasing trend of ERA5 at −5.77 W/m²/year is observed in the SSP5-8.5 scenario at −2.37 W/m²/year. Over the ten-year period, the closest average to the ERA5 WPD 898.93 W/m² at ST.1 station is observed as 710.51 W/m² under the SSP5-7.0 scenario. In the Balearic Basin (ST.2), the SSP3-7.0 scenario

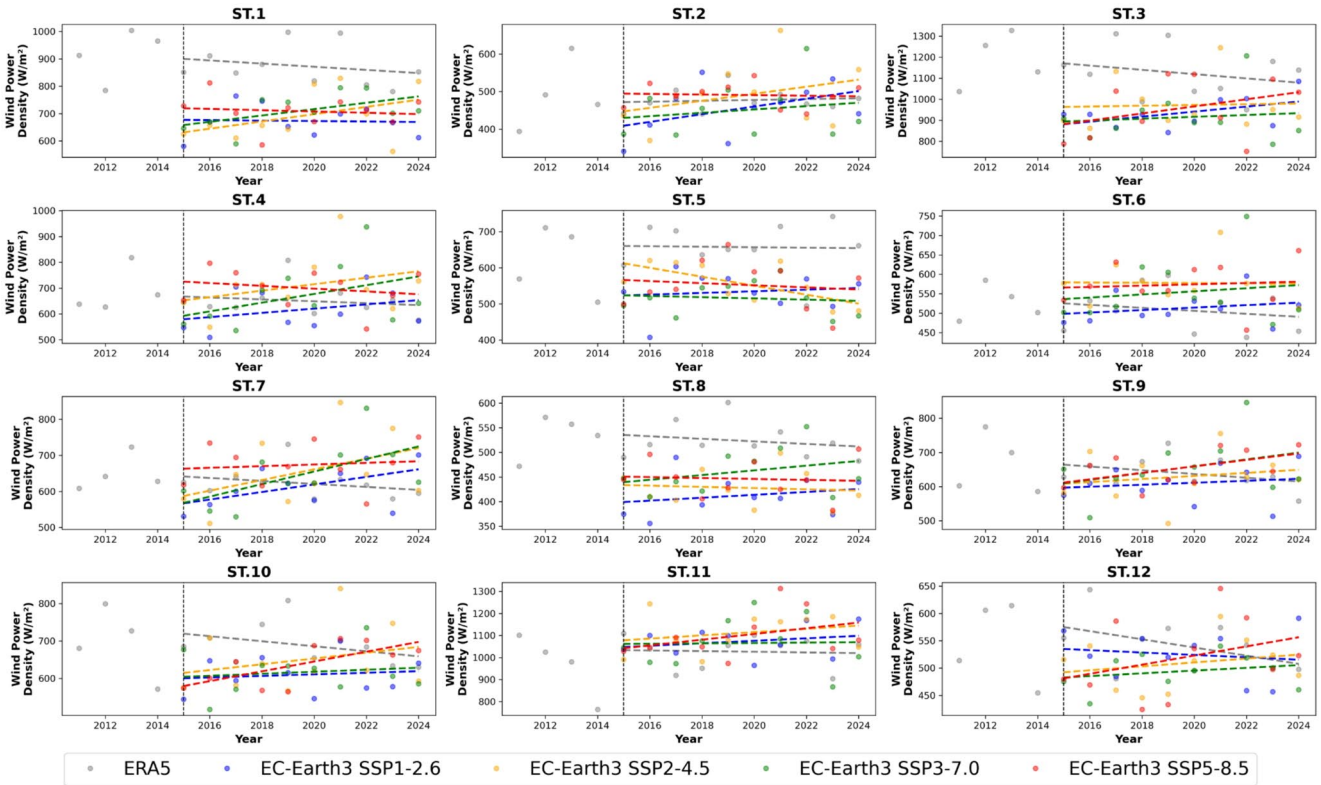


Fig. 8 Near term (2015–2024) divergence between ERA5 and EC-Earth3 future scenarios for annual mean wind power density

demonstrates a positive trend of +4.48 W/m²/year, similar to the increasing trend of +1.15 W/m²/year. Despite demonstrating a decreasing trend at ST.2, SSP5-8.5 scenario exhibits the closest average to ERA5 (492.03 W/m²) with 491.03 W/m². At ST.3, ST.7, ST.9, ST.10 and ST.11 stations, the positive trends exhibited by all SSP scenarios are in opposition to the negative trends observed in ERA5. At ST.3, ST.9 and ST.10 stations where the trends of the SSP scenarios are opposite to the ERA5 trends, the SSP2-4.5 scenario provides the closest averages (971.54 W/m², 628.66 W/m² and 649.30 W/m², respectively) to the ERA5 WPD averages, 1120.67 W/m², 636.53 W/m² and 686.87 W/m², respectively. At ST.7, most similar WPD average to ERA5 (625.15 W/m²) is evident in SSP1-2.6 scenario (614.01 W/m²). In the Aegean Basin (ST.11), SSP3-7.0 scenario shows the most similar average to ERA5 (988.32 W/m²) with 1065.64 W/m².

The sole scenario demonstrating a congruent trend direction with ERA5, displaying a decreasing trend of −3.67 W/m²/year at ST.4, is SSP5-8.5 with −5.42 W/m²/year. At this station, the SSP1-2.6 (616.13 W/m²) and SSP3-7.0 (668.79 W/m²) scenarios exhibit the closest proximity to the ERA5 WPD average (641.67 W/m²). Of the three scenarios demonstrating a decreasing trend in the Ligurian Basin (ST.5), the slightly negative trend of ERA5 (−0.68 W/m²/year) closely corresponds to the SSP3-7.0 scenario (−1.70 W/m²/year). At ST.5, the closest average to ERA5 (660.11 W/m²) is observed in the SSP2-4.5 scenario (556.64 W/m²). Contrary to the increasing trend exhibited by all other SSP scenarios in the Tyrrhenian Basin, SSP2-4.5 demonstrates a decreasing trend of −0.29 W/m²/year, aligning with the direction of ERA5 (−3.82 W/m²/year). SSP1-2.6 has an average of 512.73 W/m², which is almost exactly equal to the ERA5 WPD average (512.80 W/m²) at ST.6. The SSP2-4.5 (−1.24 W/m²/year) and SSP5-8.5 (−0.94 W/m²/year) scenarios demonstrate a congruent trend, exhibiting a decrease in WPD in the Adriatic Basin as indicated by the ERA5 (−2.60 W/m²/year). At ST.8, the most similar average to the ERA5 in WPD (519.14 W/m²) is observed in the SSP3-7.0 scenario (461.04 W/m²). SSP1-2.6 is the sole scenario that exhibits projections in the same direction (−2.18 W/m²/year) as ERA5 WPD trend (−7.49 W/m²/year) in the east of the Eastern-Mediterranean Basin. At ST.12, the scenario that shows the closest correspondence with the ERA5 WPD average (559.32 W/m²) is SSP1-2.6 (525.15 W/m²), as observed in the trend.

Near-term (2015–2024) WS and WPD projections show scenario-dependent and regionally variable changes across the Mediterranean. Under SSP5-8.5, EC-Earth3 projections generally aligned better with ERA5 trends in several basins (e.g., Alboran, Tyrrhenian, and Aegean), reflecting its superior historical performance demonstrated in Sect. 4.2. However, notable discrepancies emerged in other regions, such as the Ionian Basin (ST.9) and eastern Mediterranean (ST.10), where all SSP scenarios projected increasing trends contrary to ERA5's declining trends. These regional divergences likely stem from local atmospheric dynamics and ocean-atmosphere interactions not uniformly captured across CMIP6 models.

Unlike previous Mediterranean studies using CMIP5 RCP scenarios (Carvalho et al. 2017; Gumuscu et al. 2024; Rusu 2024), our SSP-based analysis incorporates updated socioeconomic pathways and land-use changes. The modest inter-scenario differences observed for 2015–2024 are consistent with Martinez and Iglesias (2023) for European waters, as emission pathway divergence primarily manifests in the latter half of the 21 st century. However, SSP5-8.5 already shows signals of amplified WPD changes in some northern sub-basins, suggesting early climate change impacts on wind resources.

Importantly, our direct comparison between observed ERA5 trends and SSP projections at sub-basin scales not previously conducted in Mediterranean CMIP6 studies (Carvalho et al. 2021; Claro et al. 2023; Martinez and Iglesias 2023) reveals both areas of agreement and statistically significant divergence. This highlights the need for caution when extrapolating basin-wide projections without considering local model accuracy and scenario uncertainty, particularly for near-term renewable energy planning and investment decisions.

Conclusions

This study examines the performance of 22 CMIP6 models in simulating wind climate data and their accuracy in estimating wind power density across the Mediterranean Sea. The research is important for understanding how climate change may affect offshore wind energy potential and for informing adaptation strategies. The models' wind speed and wind power density outputs were compared against ERA5 reanalysis data. The best-performing models were identified based on their precision in reproducing long-term historical wind speed averages with narrow confidence intervals. Additionally, their reliability in predicting wind power density was tested across different wind conditions from low to high energy outputs using percentile-based analysis. The results of this study allows us to identify a number of valuable conclusions.

Among the 22 CMIP6 climate models, the wind simulation data derived from the EC-Earth3 model best match ERA5 wind data across the majority of the Mediterranean sub-basins. In addition to the EC-Earth3 model, the CNRM-CM6-1-HR model showed good performance in basins with

complex morphology, such as the Adriatic Sea, the Aegean Sea, and the Ligurian Basin, with better performance compared to EC-Earth3 in the Alboran Basin. In terms of the performance of the EC-Earth3 and CNRM-CM6-1-HR models in estimating wind speeds and wind energy, the EC-Earth3 model demonstrated better performance and lower uncertainty. The EC-Earth3 model shows more stable normalized biases as a function of wind speed based on percentile evaluation. This balance ensures better future projections of wind energy related under climate change, especially in cases of increasing or decreasing extreme events in favor of low wind speed events. In other words, in the case of increased storm frequency in the future, a model that presents strong biases and high uncertainty in estimating high wind speed events will lead to greater uncertainty.

Across all 12 Mediterranean sub-regions, the scenario-dependent uncertainties in EC-Earth3 remain small in the near-term period. The bias ranges and 95% confidence intervals derived from the Welch t-tests show that differences among SSP1-2.6, SSP2-4.5, SSP3-7.0, and SSP5-8.5 are typically within ±0.2 m/s for mean wind speed and < 80 W/m² for WPD, with no systematic scenario-driven trend. Statistically significant biases, mainly in regions with stronger mesoscale wind features (e.g., ST.1, ST.3, ST.8, ST.10, ST.12), highlight where model limitations dominate over scenario effects. For most regions, however, the confidence intervals overlap across scenarios, indicating that internal variability, rather than scenario forcing, governs the near-term error spread. These results demonstrate that EC-Earth3 reproduces the regional wind climate reasonably well, but the reported bias ranges and confidence intervals should be considered when interpreting future projections.

Regarding the near-term trends, both ERA5 and EC-Earth3 SSP outputs show weak near-term (2015–2024) trends in mean wind speed. Slight positive trends were found mainly in the Alboran Basin (ST.1), southern Algerian Basin (ST.4), and Tunisian Shelf (ST.7) under some scenarios, while most other regions showed stable or slightly negative tendencies. These small and scattered signals suggest that wind conditions have remained largely unchanged, and that any apparent increases are more likely related to internal climate variability than to external forcing.

WPD trends generally follow wind speed patterns but with larger amplitude. Positive WPD trends appeared in a few sub-basins notably the Algerian (ST.3–ST.4), Tunisian Shelf (ST.7), and Aegean (ST.11) regions indicating potential localized energy variations. However, most areas, including the Adriatic (ST.8) and Eastern Mediterranean (ST.10–ST.12), showed weak or negative trends, consistent with stable to slightly declining winds in ERA5.

No systematic differences were found among SSP1-2.6, SSP2-4.5, SSP3-7.0, and SSP5-8.5 scenarios, confirming that observed short-term variations primarily reflect internal climate variability rather than scenario-driven forcing differences, as radiative forcing remains minimal during this period (IPCC 2021). EC-Earth3 realistically reproduces the observed spatial and temporal variability in ERA5, supporting its reliability for regional wind assessment, although longer evaluation periods (post-2030) would be needed to better distinguish forced changes from internal variability. The conclusions reached in this study will facilitate the selection of climate models for a regional wind research study or project in the Mediterranean Sea. Reliable model selection enables energy planners and decision makers to make more accurate offshore wind resource projections for long-term investment decisions and for an adaptation to future climate change. Furthermore, an accurate wind model can allow more accurate wave climate projections, which is important for offshore and coastal projects.

Acknowledgements The authors gratefully acknowledge the World Climate Research Programme's Working Groups responsible for CMIP6 and the contributing institutions listed in Table 1 for developing and providing access to the climate model data. We also thank the European Centre for Medium-Range Weather Forecasts (ECMWF) for supplying the ERA5 reanalysis datasets.Emre Çalışır acknowledges support from the Scientific and Technological Research Council of Turkey (TÜBİTAK) through the 2211-A National Doctoral Scholarship Program, and from the Council of Higher Education (YÖK) through the 100/2000 Doctoral Scholarship Program.

Authors' contributions Emre Çalışır: Data curation, Formal analysis, Investigation, Methodology, Software, Visualization, Writing – original draft. Khalid Amarouche: Formal analysis, Investigation, Methodology, Software, Visualization, Writing – original draft. Recep Emre Çakmak: Formal analysis, Investigation, Methodology, Software, Visualization, Writing – original draft. Adem Akpınar: Conceptualization, Supervision, Writing – review & editing.

Data availability Data will be made available on request.

Declarations

Competing interests The authors declare no competing interests.

Open Access This article is licensed under a Creative Commons Attribution-NonCommercial-NoDerivatives 4.0 International License, which permits any non-commercial use, sharing, distribution and reproduction in any medium or format, as long as you give appropriate credit to the original author(s) and the source, provide a link to the Creative Commons licence, and indicate if you modified the licensed material. You do not have permission under this licence to share adapted material derived from this article or parts of it. The images or other third party material in this article are included in the article's Creative Commons licence, unless indicated otherwise in a credit line to the material. If material is not included in the article's Creative Commons licence and your intended use is not permitted by statutory regulation or exceeds the permitted use, you will need to obtain permission directly from the copyright holder. To view a copy of this licence, visit http://creativecommons.org/licenses/by-nc-nd/4.0/.

References

Akinsanola AA, Ogunjobi KO, Abolude AT, Sarris SC, Ladipo KO (2017) Assessment of Wind Energy Potential for Small Communities in South-South Nigeria: Case Study of Koluama, Bayelsa State. J Fundamentals Renew Energy Appl 07(02). https://doi.org/10.4172/2090-4541.1000227

Akinsanola AA, Ogunjobi KO, Abolude AT, Salack S (2021) Projected changes in wind speed and wind energy potential over West Africa in CMIP6 models. Environ Res Lett 16(4):044033. https://doi.org/10.1088/1748-9326/abed7a

Akpınar A (2013) Evaluation of wind energy potentiality at coastal locations along the north eastern coasts of Turkey. Energy 50:395–405. https://doi.org/10.1016/j.energy.2012.11.019

Barbariol F, Davison S, Falcieri FM, Ferretti R, Ricchi A, Sclavo M, Benetazzo A (2021) Wind waves in the Mediterranean Sea: an ERA5 reanalysis wind-based climatology. Front Mar Sci 8:760614. https://doi.org/10.3389/fmars.2021.760614

Barcikowska MJ, Kapnick SB, Krishnamurty L, Russo S, Cherchi A, Folland CK (2020) Changes in the future summer Mediterranean climate: contribution of teleconnections and local factors. Earth Syst Dyn 11(1):161–181. https://doi.org/10.5194/esd-11-161-2020

Belmonte Rivas M, Stoffelen A (2019) Characterizing ERA-Interim and ERA5 surface wind biases using ASCAT. Ocean Sci 15(3):831–852. https://doi.org/10.5194/os-15-831-2019

Betz A (1926) Wind-Energie und Ihre Ausnutzung durch Windmühlen. Vandenhoeck & Ruprecht

Boucher O, Denvil S, Levavasseur G, Cozic A, Caubel A, Foujols M-A, Meurdesoif Y, Cadule P, Devilliers M, Ghattas J, Lebas N, Lurton T, Mellul L, Musat I, Mignot J, Cheruy F (2018) IPSL IPSL-CM6A-LR model output prepared for CMIP6 CMIP (Version 20230220) [Application/x-netcdf]. Earth System Grid Federation. https://doi.org/10.22033/ESGF/CMIP6.1534

Brune S, Olonscheck D, Suárez-Gutiérrez L, Schupfner M, Wachsmann F, Wieners K-H, Steger C, Bittner M, Jungclaus J, Früh B, Pankatz K, Giorgetta M, Reick C, Legutke S, Esch M, Gayler V, Haak H, de Vrese P, Raddatz T, Roeckner E (2022) CMIP6 CMIP MPI-ESM1-2-LR historical—RCM-forcing data (Version 1, p. 16301347920885 Bytes) [Application/x-gzip]. World Data Center for Climate (WDCC) at DKRZ. https://doi.org/10.26050/WDCC/RCM_CMIP6_HISTORICAL-LR

Brunner L, Pendergrass AG, Lehner F, Merrifield AL, Lorenz R, Knutti R (2020) Reduced global warming from CMIP6 projections when weighting models by performance and independence. Earth Syst Dyn 11(4):995–1012. https://doi.org/10.5194/esd-11-995-2020

Byun Y-H, Lim Y-J, Sung HM, Kim J, Sun M, Kim B-H (2019) NIMS-KMA KACE1.0-G model output prepared for CMIP6 CMIP historical (Version 20220928) [Application/x-netcdf]. Earth System Grid Federation. https://doi.org/10.22033/ESGF/CMIP6.8378

Çakmak RE, Çalışır E, Lemos G, Akpınar A, Semedo A, Cardoso RM, Soares PMM (2022) Evaluation of the performance of a dynamic wave climate ensemble simulated using with EURO-CORDEX winds in the Black Sea and Sea of Azov. Int J Climatol 42(16):8345–8367. https://doi.org/10.1002/joc.7711

Çakmak RE, Çalışır E, Lemos G, Akpınar A, Semedo A, Cardoso RM, Soares PMM (2023) Regional wave climate projections forced by EURO-CORDEX winds for the Black Sea and Sea of Azov towards the end of the 21st century. Int J Climatol 43(13):5927–5950. https://doi.org/10.1002/joc.8181

Çakmak RE, Amarouche K, Akpınar A, Otay EN (2025) Projected changes in wave storm patterns near key ports and shipping routes in the Black Sea. Ocean Coast Manage 261:107537. https://doi.org/10.1016/j.ocecoaman.2024.107537

Çalışır E, Soran MB, Akpınar A (2023) Quality of the ERA5 and CFSR winds and their contribution to wave modelling performance in a semi-closed sea. J Oper Oceanogr 16(2):106–130. https://doi.org/10.1080/1755876X.2021.1911126

Campins J, Genovés A, Picornell MA, Jansà A (2011) Climatology of Mediterranean cyclones using the ERA-40 dataset. Int J Climatol 31(11):1596–1614. https://doi.org/10.1002/joc.2183

Cao J, Wang B (2019) NUIST NESMv3 model output prepared for CMIP6 CMIP (Version 20230720) [Application/x-netcdf]. Earth System Grid Federation. https://doi.org/10.22033/ESGF/CMIP6.2021

Carrasco CA, Landsea CW, Lin Y-L (2014) The influence of tropical cyclone size on its intensification. Weather Forecast 29(3):582–590. https://doi.org/10.1175/WAF-D-13-00092.1

Carvalho D, Rocha A, Gómez-Gesteira M, Silva Santos C (2017) Potential impacts of climate change on European wind energy resource under the CMIP5 future climate projections. Renew Energy 101:29–40. https://doi.org/10.1016/j.renene.2016.08.036

Carvalho D, Rocha A, Costoya X, deCastro M, Gómez-Gesteira M (2021) Wind energy resource over Europe under CMIP6 future climate projections: what changes from CMIP5 to CMIP6. Renew Sustain Energy Rev 151:111594. https://doi.org/10.1016/j.rser.2021.111594

Çetin II, Yücel I, Yılmaz MT, Önol B (2024) Historical variability of Coupled Model Intercomparison Project Version 6 (CMIP6)-driven surface winds and global reanalysis data for the Eastern Mediterranean. Theor Appl Climatol 155(5):4101–4121. https://doi.org/10.1007/s00704-024-04869-y

Chirosca A-M, Rusu L (2025) Projections of wind and wave climate on the main routes of the Mediterranean and Black Seas. J Ocean Eng Mar Energy 11(1):149–167. https://doi.org/10.1007/s40722-024-00375-5

Claro A, Santos JA, Carvalho D (2023) Assessing the Future wind Energy Potential in Portugal Using a CMIP6 Model Ensemble and WRF High-Resolution Simulations. Energies 16(2):661. https://doi.org/10.3390/en16020661

Cos Espuna J (2021) Mediterranean climate change projections from CMIP5 and CMIP6 [Master's Thesis]. Universitat de Barcelona

Cramer W, Guiot J, Fader M, Garrabou J, Gattuso J-P, Iglesias A, Lange MA, Lionello P, Llasat MC, Paz S, Peñuelas J, Snoussi M, Toreti A, Tsimplis MN, Xoplaki E (2018) Climate change and interconnected risks to sustainable development in the Mediterranean. Nat Clim Change 8(11):972–980. https://doi.org/10.1038/s41558-018-0299-2

Dahunsi AM, Bonou F, Dada OA, Baloïtcha E (2025) Quantifying climate change-driven variations in projected wind condition in the Gulf of Guinea. Dyn Atmos Oceans 110:101543. https://doi.org/10.1016/j.dynatmoce.2025.101543

Decremer D, Chung CE, Ekman AML, Brandefelt J (2014) Which significance test performs the best in climate simulations? Tellus A Dyn Meteorol Oceanogr 66(1):23139. https://doi.org/10.3402/tellusa.v66.23139

Dix M, Bi D, Dobrohotoff P, Fiedler R, Harman I, Law R, Mackallah C, Marsland S, O'Farrell S, Rashid H, Srbinovsky J, Sullivan A, Trenham C, Vohralik P, Watterson I, Williams G, Woodhouse M, Bodman R, Dias FB, Yang R (2019) CSIRO-ARCCSS ACCESS-CM2 model output prepared for CMIP6 ScenarioMIP ssp245 (Version 20230720) [Application/x-netcdf]. Earth System Grid Federation. https://doi.org/10.22033/ESGF/CMIP6.4321

Dong X, Wang Y, Hou S, Ding M, Yin B, Zhang Y (2020) Robustness of the Recent Global Atmospheric Reanalyses for Antarctic Near-Surface Wind Speed Climatology. J Clim 33(10):4027–4043. https://doi.org/10.1175/JCLI-D-19-0648.1

Drobinski P, Ducrocq V, Alpert P, Anagnostou E, Béranger K, Borga M, Braud I, Chanzy A, Davolio S, Delrieu G, Estournel C, Boubrahmi NF, Font J, Grubišić V, Gualdi S, Homar V, Ivančan-Picek B, Kottmeier C, Kotroni V, Wernli H (2014) HyMeX: a 10-year multidisciplinary program on the Mediterranean water cycle. Bull

Am Meteorol Soc 95(7):1063–1082. https://doi.org/10.1175/BAMS-D-12-00242.1
EC-Earth (2019) EC-Earth-Consortium EC-Earth3 model output prepared for CMIP6 ScenarioMIP ssp585 (Version 20230720) [Application/x-netcdf]. https://doi.org/10.22033/ESGF/CMIP6.4912. Earth System Grid Federation
Emeis S (2005) How well does a power law fit to a diabatic boundary-layer wind profile? https://doi.org/10.5445/IR/120060755
Emeis S (2013) Wind Energy Meteorology: Atmospheric Physics for Wind Power Generation. Springer, Berlin Heidelberg. https://doi.org/10.1007/978-3-642-30523-8
ESGF (2024) Earth System Grid Federation CMIP6 data repository. https://esgf-node.llnl.gov/search/cmip6/
Eyring V, Bony S, Meehl GA, Senior CA, Stevens B, Stouffer RJ, Taylor KE (2016) Overview of the Coupled Model Intercomparison Project Phase 6 (CMIP6) experimental design and organization. Geosci Model Dev 9(5):1937–1958. https://doi.org/10.5194/gmd-9-1937-2016
Gidden MJ, Riahi K, Smith SJ, Fujimori S, Luderer G, Kriegler E, Van Vuuren DP, Van Den Berg M, Feng L, Klein D, Calvin K, Doelman JC, Frank S, Fricko O, Harmsen M, Hasegawa T, Havlik P, Hilaire J, Hoesly R, Takahashi K (2019) Global emissions pathways under different socioeconomic scenarios for use in CMIP6: a dataset of harmonized emissions trajectories through the end of the century. Geosci Model Dev 12(4):1443–1475. https://doi.org/10.5194/gmd-12-1443-2019
Gohari A, Akpinar A (2024) Projected Changes in Wind Speed and Wind Energy Resources Over the Persian Gulf Based on Bias Corrected Cmip6 Models. https://doi.org/10.2139/ssrn.5036638
Gumuscu I, Sahin C, Yuksel Y, Arı Güner HA, Islek F (2024) Evaluation of future wind climate over the Eastern Mediterranean Sea. Reg Stud Mar Sci 78:103780. https://doi.org/10.1016/j.rsma.2024.103780
Gutjahr O, Putrasahan D, Lohmann K, Jungclaus JH, Von Storch J-S, Brüggemann N, Haak H, Stössel A (2019) Max Planck Institute Earth System Model (MPI-ESM1.2) for the High-Resolution Model Intercomparison Project (HighResMIP). Geosci Model Dev 12(7):3241–3281. https://doi.org/10.5194/gmd-12-3241-2019
Hdidouan D, Staffell I (2017) The impact of climate change on the levelised cost of wind energy. Renew Energy 101:575–592. https://doi.org/10.1016/j.renene.2016.09.003
Hersbach H, de Rosnay P, Bell B, Schepers D, Simmons A, Soci C, Abdalla S, Alonso-Balmaseda M, Balsamo G, Bechtold P, Berrisford P, Bidlot J-R, de Boisséson E, Bonavita M, Browne P, Buizza R, Dahlgren P, Dee D, Dragani R, Zuo H (2018) Operational global reanalysis: Progress, future directions and synergies with NWP. https://doi.org/10.21957/TKIC6G3WM
Hersbach H, Bell B, Berrisford P, Hirahara S, Horányi A, Muñoz-Sabater J, Nicolas J, Peubey C, Radu R, Schepers D, Simmons A, Soci C, Abdalla S, Abellan X, Balsamo G, Bechtold P, Biavati G, Bidlot J, Bonavita M, Thépaut J (2020) The ERA5 global reanalysis. Q J R Meteorol Soc 146(730):1999–2049. https://doi.org/10.1002/qj.3803
IEC 61400-1 (2019) IEC 61400-1: Wind energy generation systems—Part 1: Design requirements (International Standard 61400; Version 1). https://webstore.iec.ch/en/publication/26423
IPCC (2021) Climate Change 2021 – The Physical Science Basis: Working Group I Contribution to the Sixth Assessment Report of the Intergovernmental Panel on Climate Change, 1st edn. Cambridge University Press. https://doi.org/10.1017/9781009157896
IPCC (Ed.) (2001) Climate change 2001: The scientific basis. Cambridge univ. press
IRENA (2023) Renewable Power Generation Costs in 2023. International Renewable Energy Agency
Juckes M, Taylor KE, Durack PJ, Lawrence B, Mizielinski MS, Pamment A, Peterschmitt J-Y, Rixen M, Sénési S (2020) The CMIP6 data request (DREQ, version 01.00.31). Geosci Model Dev 13(1):201–224. https://doi.org/10.5194/gmd-13-201-2020
Kamranzad B, Mori N (2019) Future wind and wave climate projections in the Indian Ocean based on a super-high-resolution MRI-AGCM3.2S model projection. Clim Dyn 53(3–4):2391–2410. https://doi.org/10.1007/s00382-019-04861-7
Kamranzad B, Tatebe H, Takara K (2020a) Multi-decadal variability in global wind and wave climate: An analysis based on miroc6 dataset. Creating Resil Water-Related Challenges, 1–4
Kamranzad B, Tatebe H, Takara K (2020b) Spatio-temporal assessment of long-term historical wave simulation using MIROC6 wind dataset; A global scale study. Ocean Sciences Meeting 2020, San Diego, California
Kendall M (1975) Rank Correlation Methods, 4th edition. Charles Griffin
Kim Y, Noh Y, Kim D, Lee M-I, Lee HJ, Kim SY, Kim D (2019) KIOST KIOST-ESM model output prepared for CMIP6 CMIP (Version 20230720) [Application/x-netcdf]. Earth System Grid Federation. https://doi.org/10.22033/ESGF/CMIP6.1922
Knutti R, Furrer R, Tebaldi C, Cermak J, Meehl GA (2010) Challenges in combining projections from multiple climate models. J Clim 23(10):2739–2758. https://doi.org/10.1175/2009JCLI3361.1
Krishnan A, Bhaskaran PK (2020) Skill assessment of global climate model wind speed from CMIP5 and CMIP6 and evaluation of projections for the Bay of Bengal. Clim Dyn 55(9–10):2667–2687. https://doi.org/10.1007/s00382-020-05406-z
Lemos G, Semedo A, Dobrynin M, Menendez M, Miranda PMA (2020) Bias-corrected CMIP5-derived single-forcing future wind-wave climate projections toward the end of the twenty-first century. J Appl Meteorol Climatol 59(9):1393–1414. https://doi.org/10.1175/JAMC-D-19-0297.1
Lemos G, Semedo A, Kumar R, Dobrynin M, Akpinar A, Kamranzad B, Bidlot J, Lobeto H (2023) Performance evaluation of a global CMIP6 single forcing, multi wave model ensemble of wave climate simulations. Ocean Model 184:102237. https://doi.org/10.1016/j.ocemod.2023.102237
Lionello P, Scarascia L (2018) The relation between climate change in the Mediterranean region and global warming. Reg Environ Change 18(5):1481–1493. https://doi.org/10.1007/s10113-018-1290-1
Lionello P, Bhend J, Buzzi A, Della-Marta PM, Krichak SO, Jansà A, Maheras P, Sanna A, Trigo IF, Trigo R (2006) Chapter 6 Cyclones in the Mediterranean region: Climatology and effects on the environment. In Developments in Earth and Environmental Sciences (Vol. 4, pp. 325–372). Elsevier. https://doi.org/10.1016/S1571-9197(06)80009-1
Lira-Loarca A, Ferrari F, Mazzino A, Besio G (2021) Future wind and wave energy resources and exploitability in the Mediterranean Sea by 2100. Appl Energy 302:117492. https://doi.org/10.1016/j.apenergy.2021.117492
Lobeto H, Menendez M, Losada IJ (2021) Future behavior of wind wave extremes due to climate change. Sci Rep 11(1):7869. https://doi.org/10.1038/s41598-021-86524-4
Lobeto H, Semedo A, Menendez M, Lemos G, Kumar R, Akpinar A, Dobrynin M, Kamranzad B (2023) On the assessment of the wave modeling uncertainty in wave climate projections. Environ Res Lett 18(12):124006. https://doi.org/10.1088/1748-9326/ad0137
Lovato T, Peano D (2020) CMCC CMCC-CM2-SR5 model output prepared for CMIP6 ScenarioMIP ssp585 (Version 20230720) [Application/x-netcdf]. https://doi.org/10.22033/ESGF/CMIP6.3896. Earth System Grid Federation
Mann HB (1945) Nonparametric tests against trend. Econometrica 13(3):245. https://doi.org/10.2307/1907187

Manwell JF, McGowan JG, Rogers AL (2009) Wind Energy Explained: Theory, Design and Application (1st ed.). Wiley. https://doi.org/10.1002/9781119994367

Martinez A, Iglesias G (2023) Climate-change impacts on offshore wind resources in the Mediterranean Sea. Energy Convers Manag 291:117231. https://doi.org/10.1016/j.enconman.2023.117231

Mohan S, Bhaskaran PK (2019) Evaluation and bias correction of global climate models in the CMIP5 over the Indian Ocean region. Environ Monit Assess 191(S3):806. https://doi.org/10.1007/s10661-019-7700-0

Morim J, Hemer M, Wang XL, Cartwright N, Trenham C, Semedo A, Young I, Bricheno L, Camus P, Casas-Prat M, Erikson L, Mentaschi L, Mori N, Shimura T, Timmermans B, Aarnes O, Breivik Ø, Behrens A, Dobrynin M, Andutta F (2019) Robustness and uncertainties in global multivariate wind-wave climate projections. Nat Clim Change 9(9):711–718. https://doi.org/10.1038/s41558-019-0542-5

Narayanasetti S, Panickal S, Raghavan K, Gopinathan PA, Choudhury AD, Singh M (2019) CCCR-IITM IITM-ESM model output prepared for CMIP6 CMIP piControl (Version 20230720) [Application/x-netcdf]. https://doi.org/10.22033/ESGF/CMIP6.3710. Earth System Grid Federation

NASA/GISS (2018) NASA-GISS GISS-E2.1G model output prepared for CMIP6 CMIP (Version 20230720) [Application/x-netcdf]. Earth System Grid Federation. https://doi.org/10.22033/ESGF/CMIP6.1400

Neill SP (2024) Wave resource characterization and co-location with offshore wind in the Irish Sea. Renew Energy 222:119902. https://doi.org/10.1016/j.renene.2023.119902

Neubauer D, Ferrachat S, Siegenthaler-Le Drian C, Stoll J, Folini DS, Tegen I, Wieners K-H, Mauritsen T, Stemmler I, Barthel S, Bey I, Daskalakis N, Heinold B, Kokkola H, Partridge D, Rast S, Schmidt H, Schutgens N, Stanelle T, Lohmann U (2019) HAM-MOZ-Consortium MPI-ESM1.2-HAM model output prepared for CMIP6 AerChemMIP (Version 20230319) [Application/x-netcdf]. Earth System Grid Federation. https://doi.org/10.22033/ESGF/CMIP6.1621

Nissen KM, Leckebusch GC, Pinto JG, Renggli D, Ulbrich S, Ulbrich U (2010) Cyclones causing wind storms in the Mediterranean: characteristics, trends and links to large-scale patterns. Nat Hazards Earth Syst Sci 10(7):1379–1391. https://doi.org/10.5194/nhess-10-1379-2010

O'Neill BC, Tebaldi C, Van Vuuren DP, Eyring V, Friedlingstein P, Hurtt G, Knutti R, Kriegler E, Lamarque J-F, Lowe J, Meehl GA, Moss R, Riahi K, Sanderson BM (2016) The Scenario Model Intercomparison Project (ScenarioMIP) for CMIP6. Geosci Model Dev 9(9):3461–3482. https://doi.org/10.5194/gmd-9-3461-2016

Peano D, Lovato T, Materia S (2020) CMCC CMCC-ESM2 model output prepared for CMIP6 LS3MIP (Version 20230213) [Application/x-netcdf]. https://doi.org/10.22033/ESGF/CMIP6.13165. Earth System Grid Federation

Pryor SC, Barthelmie RJ, Young DT, Takle ES, Arritt RW, Flory D, Gutowski WJ, Nunes A, Roads J (2009) Wind speed trends over the contiguous United States. J Geophys Res Atmos 114(D14):2008JD011416. https://doi.org/10.1029/2008JD011416

Reyers M, Moemken J, Pinto JG (2016) Future changes of wind energy potentials over Europe in a large CMIP5 multi-model ensemble. Int J Climatol 36(2):783–796. https://doi.org/10.1002/joc.4382

Ridley J, Menary M, Kuhlbrodt T, Andrews M, Andrews T (2019a) MOHC HadGEM3-GC31-LL model output prepared for CMIP6 CMIP historical (Version 20230220) [Application/x-netcdf]. https://doi.org/10.22033/ESGF/CMIP6.6109. Earth System Grid Federation

Ridley J, Menary M, Kuhlbrodt T, Andrews M, Andrews T (2019b) MOHC HadGEM3-GC31-MM model output prepared for CMIP6 CMIP historical (Version 20230720) [Application/x-netcdf]. https://doi.org/10.22033/ESGF/CMIP6.6112. Earth System Grid Federation

Rusu E (2024) The expected wind power dynamics in the Mediterranean Sea considering different climate change scenarios. Renew Energy 227:120500. https://doi.org/10.1016/j.renene.2024.120500

Rusu L (2025) Climate change impact on the sea state conditions in the Mediterranean Sea under RCP and SSP emission scenarios. Renew Energy 243:122616. https://doi.org/10.1016/j.renene.2025.122616

Ruxton GD (2006) The unequal variance t-test is an underused alternative to Student's t-test and the Mann–Whitney U test. Behav Ecol 17(4):688–690. https://doi.org/10.1093/beheco/ark016

Samuels R, Hochman A, Baharad A, Givati A, Levi Y, Yosef Y, Saaroni H, Ziv B, Harpaz T, Alpert P (2018) Evaluation and projection of extreme precipitation indices in the Eastern Mediterranean based on CMIP5 multi-model ensemble. Int J Climatol 38(5):2280–2297. https://doi.org/10.1002/joc.5334

Sanderson BM, Wehner M, Knutti R (2017) Skill and independence weighting for multi-model assessments. Geosci Model Dev 10(6):2379–2395. https://doi.org/10.5194/gmd-10-2379-2017

Sawadogo W, Abiodun BJ, Okogbue EC (2019) Projected changes in wind energy potential over West Africa under the global warming of 1.5°C and above. Theor Appl Climatol 138(1–2):321–333. https://doi.org/10.1007/s00704-019-02826-8

Schulzweida U (2023) CDO User Guide. https://doi.org/10.5281/ZENODO.10020800

Semedo A, Sušelj K, Rutgersson A, Sterl A (2011) A global view on the wind sea and swell climate and variability from ERA-40. J Clim 24(5):1461–1479. https://doi.org/10.1175/2010JCLI3718.1

Semedo A, Weisse R, Behrens A, Sterl A, Bengtsson L, Günther H (2012) Projection of global wave climate change toward the end of the twenty-first century. J Clim 26(21):8269–8288. https://doi.org/10.1175/JCLI-D-12-00658.1

Semmler T, Danilov S, Rackow T, Sidorenko D, Barbi D, Hegewald J, Sein D, Wang Q, Jung T (2018) AWI AWI-CM1.1MR model output prepared for CMIP6 CMIP historical (Version 20230220) [Application/x-netcdf]. Earth System Grid Federation. https://doi.org/10.22033/ESGF/CMIP6.2686

Sen PK (1968) Estimates of the regression coefficient based on Kendall's tau. J Am Stat Assoc 63(324):1379–1389. https://doi.org/10.1080/01621459.1968.10480934

Shiogama H, Abe M, Tatebe H (2019) MIROC MIROC6 model output prepared for CMIP6 ScenarioMIP ssp245 (Version 20230720) [Application/x-netcdf]. Earth System Grid Federation. https://doi.org/10.22033/ESGF/CMIP6.5746

Staffell I, Pfenninger S (2016) Using bias-corrected reanalysis to simulate current and future wind power output. Energy 114:1224–1239. https://doi.org/10.1016/j.energy.2016.08.068

Stouffer RJ, Eyring V, Meehl GA, Bony S, Senior C, Stevens B, Taylor KE (2017) CMIP5 scientific gaps and recommendations for CMIP6. Bull Am Meteorol Soc 98(1):95–105. https://doi.org/10.1175/BAMS-D-15-00013.1

Susini S, Menendez M, Eguia P, Blanco JM (2022) Climate change impact on the offshore wind energy over the North Sea and the Irish Sea. Front Energy Res 10:881146. https://doi.org/10.3389/fenrg.2022.881146

Tachiiri K, Abe M, Hajima T, Arakawa O, Suzuki T, Komuro Y, Ogochi K, Watanabe M, Yamamoto A, Tatebe H, Noguchi MA, Ohgaito R, Ito A, Yamazaki D, Ito A, Takata K, Watanabe S, Kawamiya M (2019) MIROC MIROC-ES2L model output prepared for CMIP6 ScenarioMIP (Version 20230720) [Application/x-netcdf]. Earth System Grid Federation. https://doi.org/10.22033/ESGF/CMIP6.936

Tebaldi C, Knutti R (2007) The use of the multi-model ensemble in probabilistic climate projections. Philosophical Trans Royal Soc A: Math Phys Eng Sci 365(1857):2053–2075. https://doi.org/10.1098/rsta.2007.2076

Theil H (1950) A Rank-Invariant Method of Linear and Polynomial Regression Analysis, Part I; Confidence Regions for the Parameters of Polynomial Regression Eq. 53:386–392

Toomey T, Lira-Loarca A, Marcos M, Besio G, Orfila A (2025) Future wave climate in the Mediterranean Sea and associated uncertainty from an ensemble of 31 GCM-RCM wave simulations. Earths Future 13(4):e2024EF004992. https://doi.org/10.1029/2024EF004992

Trigo IF, Davies TD, Bigg GR (1999) Objective climatology of cyclones in the Mediterranean Region. J Climate 12(6):1685–1696

Tuel A, Eltahir EAB (2020) Why Is the Mediterranean a Climate Change Hot Spot? J Clim 33(14):5829–5843. https://doi.org/10.1175/JCLI-D-19-0910.1

Voldoire A (2018) CNRM-CERFACS CNRM-CM6-1 model output prepared for CMIP6 CMIP (Version 20230720) [Application/x-netcdf]. Earth System Grid Federation. https://doi.org/10.22033/ESGF/CMIP6.1375

Voldoire A (2019) CNRM-CERFACS CNRM-CM6-1-HR model output prepared for CMIP6 CMIP (Version 20230720) [Application/x-netcdf]. Earth System Grid Federation. https://doi.org/10.22033/ESGF/CMIP6.1385

von Storch J-S, Putrasahan D, Lohmann K, Gutjahr O, Jungclaus J, Bittner M, Haak H, Wieners K-H, Giorgetta M, Reick C, Esch M, Gayler V, de Vrese P, Raddatz T, Mauritsen T, Behrens J, Brovkin V, Claussen M, Crueger T, Roeckner E (2017) MPI-M MPIESM1.2-HR model output prepared for CMIP6 HighResMIP (Version 20230720) [Application/x-netcdf]. Earth System Grid Federation. https://doi.org/10.22033/ESGF/CMIP6.762

Welch BL (1947) The Generalization of `Student's' Problem when Several Different Population Variances are Involved. Biometrika 34(1/2):28. https://doi.org/10.2307/2332510

Xin X, Zhang J, Zhang F, Wu T, Shi X, Li J, Chu M, Liu Q, Yan J, Ma Q, Wei M (2018) BCC BCC-CSM2MR model output prepared for CMIP6 CMIP (Version 20230220) [Application/x-netcdf]. Earth System Grid Federation. https://doi.org/10.22033/ESGF/CMIP6.1725

Yukimoto S, Koshiro T, Kawai H, Oshima N, Yoshida K, Urakawa S, Tsujino H, Deushi M, Tanaka T, Hosaka M, Yoshimura H, Shindo E, Mizuta R, Ishii M, Obata A, Adachi Y (2019) MRI MRI-ESM2.0 model output prepared for CMIP6 CMIP (Version 20230720) [Application/x-netcdf]. Earth System Grid Federation. https://doi.org/10.22033/ESGF/CMIP6.621

Publisher's note Springer Nature remains neutral with regard to jurisdictional claims in published maps and institutional affiliations.